JCI The Journal of Clinical Investigation

Maintenance DNA methylation is required for induced Treg reparative function following viral pneumonia in mice

Anthony M. Joudi, … , Samuel E. Weinberg, Benjamin D. Singer

J Clin Invest. 2025. https://doi.org/10.1172/JCI192925.

Research In-Press Preview Immunology Inflammation Pulmonology

Graphical abstract

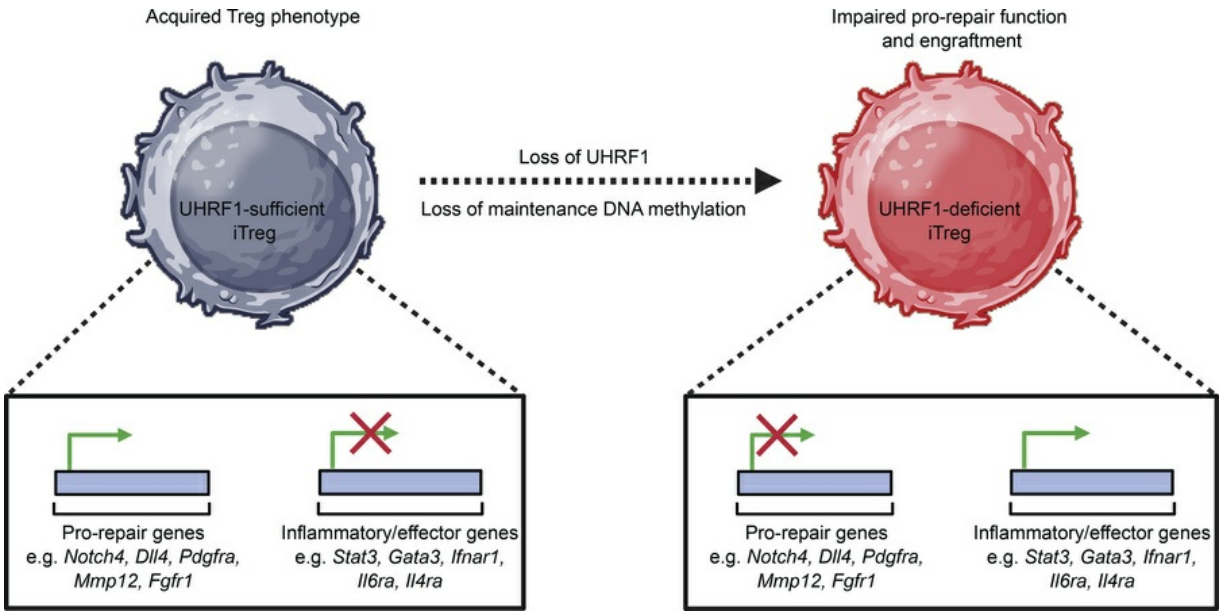

Maintenance DNA methylation is required for induced Treg reparative function following viral pneumonia in mice

Anthony M. Joudi[1], Jonathan K. Gurkan[1,2,3], Qianli Liu[1,3], Elizabeth M. Steinert[1], Manuel A. Torres Acosta[1,2,3], Kathryn A. Helmin[1], Luisa Morales-Nebreda[1], Nurbek Mambetsariev[4], Carla Patricia Reyes Flores[1,3], Hiam Abdala-Valencia[1], Samuel E. Weinberg[5], Benjamin D. Singer[1,6,7,8*]

[1]Division of Pulmonary and Critical Care Medicine, Northwestern University Feinberg School of Medicine, Chicago, IL, USA
[2]Medical Scientist Training Program, Northwestern University Feinberg School of Medicine, Chicago, IL, USA
[3]Driskill Graduate Program, Northwestern University Feinberg School of Medicine, Chicago, IL, USA
[4]Division of Allergy and Immunology, Northwestern University Feinberg School of Medicine, Chicago, IL, USA
[5]Department of Pathology, Northwestern University Feinberg School of Medicine, Chicago IL, USA
[6]Department of Biochemistry and Molecular Genetics, Northwestern University Feinberg School of Medicine, Chicago, IL, USA
[7]Simpson Querrey Institute for Epigenetics, Northwestern University Feinberg School of Medicine, Chicago, IL, USA
[8]Simpson Querrey Lung Institute for Translational Science (SQ LIFTS), Northwestern University Feinberg School of Medicine, Chicago, IL, USA

*To whom correspondence should be addressed:
Benjamin D. Singer, MD
Division of Pulmonary and Critical Care Medicine, Department of Medicine
Department of Biochemistry and Molecular Genetics
Northwestern University Feinberg School of Medicine
303 E. Superior St.
Simpson Querrey 5th Floor
Chicago, IL 60611 USA
benjamin-singer@northwestern.edu
Tel: (312) 503-4494
Fax: (312) 503-0411

Conflict of interest statement: NM is currently an employee and owns stock in Vertex Pharmaceuticals. BDS holds United States Patent No. US 10,905,706 B2, Compositions and Methods to Accelerate Resolution of Acute Lung Inflammation, and serves on the Scientific Advisory Board of Zoe Biosciences. The other authors have no competing interests to declare.

Abstract

FOXP3+ natural regulatory T cells (nTregs) promote resolution of inflammation and repair of epithelial damage following viral pneumonia-induced lung injury, thus representing a cellular therapy for patients with severe viral pneumonia and the acute respiratory distress syndrome (ARDS). Whether in vitro induced Tregs (iTregs), which can be rapidly generated in substantial numbers from conventional T cells, also promote lung recovery is unknown. nTregs require specific DNA methylation patterns maintained by the epigenetic regulator, ubiquitin-like with PHD and RING finger domains 1 (UHRF1). Here, we tested whether iTregs promote recovery following viral pneumonia and whether iTregs require UHRF1 for their pro-recovery function. We found that adoptive transfer of iTregs to mice with influenza virus pneumonia promotes lung recovery and that loss of UHRF1-mediated maintenance DNA methylation in iTregs leads to reduced engraftment and a delayed repair response. Transcriptional and DNA methylation profiling of adoptively transferred UHRF1-deficient iTregs that had trafficked to influenza-injured lungs demonstrated transcriptional instability with gain of effector T cell lineage-defining transcription factors. Strategies to promote the stability of iTregs could be leveraged to further augment their pro-recovery function during viral pneumonia and other causes of severe lung injury.

Introduction

Regulatory T cells (Tregs) are a subset of $CD4^+$ T cells that prevent spontaneous autoimmunity and mitigate exuberant immune responses by promoting self-tolerance and anergy (1,2). Tregs also promote repair in multiple tissue types, including the lungs, following acute injury due to infection or sterile triggers (3-11). To maintain their identity and function, Tregs require expression of the lineage-determining transcription factor, FOXP3, and maintenance of a signature DNA methylation landscape at key genomic elements, such as the *Foxp3* super-enhancer and other Treg-specific super-enhancers (Treg-SE) (12-14). Natural regulatory T cells (nTregs) emigrate from the thymus expressing FOXP3 and with the Treg lineage-determining DNA methylation landscape in place (12,13). These cells are relatively rare—5–15% of circulating $CD4^+$ T cells—and, unfortunately, are difficult to expand ex vivo, posing a barrier to therapeutic Treg transfer protocols (15). Induced regulatory T cells (iTregs) derive from conventional ($FOXP3^-$) $CD4^+$ T cells that express FOXP3 after culture in the presence of TGF-β, IL-2, and T cell receptor (TCR) stimulation, resulting in gain of nTreg-like suppressive functions. As iTregs are derived in vitro from conventional $CD4^+$ T cells, a more abundant cell type, they can expand more robustly and rapidly than nTregs, an attractive feature for clinical use. Whether iTregs function like nTregs to promote recovery following acute lung injury is not known. Moreover, iTregs do not carry the signature DNA methylation landscape seen in nTregs, leading to transcriptional instability in inflammatory microenvironments and potential conversion to pro-inflammatory T cell phenotypes (12,16-18). Indeed, modulation of the epigenetic landscape via DNA methyltransferase inhibition or TET enzyme activation augments the stability and function of natural and induced Tregs (8,19-25). Elucidating targetable mechanisms that stabilize iTreg transcriptional programs and function therefore represents an important objective for developing Treg-based therapies that promote recovery from severe pneumonia (15,26).

The epigenetic regulator, ubiquitin-like with PHD and RING finger domains 1 (UHRF1, also known as Np95 in mice and ICBP90 in humans), is a multidomain non-redundant adapter protein that recruits the maintenance DNA methyltransferase, DNMT1, to replicating daughter DNA strands to maintain cell type-specific methylation patterns during DNA replication (27-29). UHRF1 is required for the stability of nTreg identity; loss of UHRF1 in nTregs during thymic development or in the adult mouse leads to generation of inflammatory ex-FOXP3 (i.e., ex-Treg) cells (30). In contrast, the necessity of UHRF1 in regulating iTreg stability and function is less clear. Published data suggest that UHRF1 is dispensable

for iTreg generation (30,31), yet others have reported that iTreg generation from UHRF1-deficient conventional $CD4^+$ T cells augments their suppressive function in a colitis model of inflammation (31). We hypothesized that iTregs require UHRF1-mediated maintenance DNA methylation to stabilize their acquired transcriptional and functional programs.

To test our hypothesis, we performed adoptive transfer of UHRF1-sufficient or -deficient iTregs into Treg-depleted mice with influenza A virus pneumonia, which do not recover from lung injury in the absence of reconstitution of the Treg population. Adoptive transfer of UHRF1-sufficient iTregs promoted recovery similar to adoptive transfer of nTregs. In contrast, we found that recipients of UHRF1-deficient iTregs suffered worsened hypoxemia and mortality as well as delayed alveolar epithelial repair compared with mice that received UHRF1-sufficient iTregs. UHRF1-deficient iTregs displayed reduced lung engraftment at early and late recovery timepoints. Loss of UHRF1-mediated maintenance DNA methylation had no effect on FOXP3 induction yet resulted in a significant instability in vivo and caused significant transcriptomic instability at other core Treg loci in vitro and in vivo during viral pneumonia. In summary, UHRF1-mediated maintenance DNA methylation stabilizes iTreg cellular identity and reparative function following viral pneumonia.

Results

nTregs and iTregs promote recovery following viral pneumonia.

Transient depletion of FOXP3$^+$ nTregs is followed by a renewal of the FOXP3$^+$ population (32). To determine when after viral infection FOXP3$^+$ Tregs promote recovery and optimize the timing of Treg adoptive transfer, we first assessed whether the timing of Treg renewal determines influenza pneumonia recovery phenotypes. To deplete Tregs, we administered loading doses of diphtheria toxin (DTx) to *Foxp3*$^{GFP\text{-}DTR}$ mice two days prior to sublethal influenza A virus infection and continued DTx administration every two days until 6, 10, 14, or 21 days post infection (DPI) (Supplemental Figure 1A). We previously reported that DTx administration to wild-type mice with viral pneumonia does not contribute to immunopathology (33). Here, we confirmed depletion of Tregs in the spleen at 6 DPI (4 doses of DTx) in *Foxp3*$^{GFP\text{-}DTR}$ mice (Supplemental Figure 1B)**.** *Foxp3*$^{GFP\text{-}DTR}$ mice that received PBS and *Foxp3*^{Cre} mice that received DTx were included for comparison and demonstrated a typical frequency of endogenous Tregs in the spleen (Supplemental Figure 1B). An analysis of mice on 13 DPI that had DTx withdrawn on 6 DPI revealed that the Treg population in the spleen and lung were renewing, but had not yet returned to baseline, when compared to infected mice that had not received DTx (Supplemental Figure 1C). Following influenza infection, we found that *Foxp3*$^{GFP\text{-}DTR}$ mice that had DTx withdrawn at 6 DPI recovered their mass faster than mice that continued to receive DTx through 10, 14, or 21 DPI (Supplemental Figure 1D). Because administration of DTx alone results in some loss of mass (34), and thus this measure may also reflect DTx withdrawal timing rather than degree of resolving lung injury, we confirmed and compared the degree of lung injury in representative mice via histology at 60 DPI. While all groups had evidence of residual lung injury, the quantification of damaged lung tissue revealed it was most severe in mice that continued to receive DTx through 21 DPI (Supplemental Figure 1E). In response to antigen or inflammation in vivo, some conventional (FOXP3$^-$) CD4$^+$ T cells transiently express FOXP3 but not the signature DNA methylation pattern characteristic of nTregs; these cells are known as peripheral Tregs (pTregs) (35-39). Accordingly, we determined the DNA methylation profile of FOXP3$^+$ cells that repopulate following withdrawal of DTx in the influenza virus pneumonia model. Genome-wide DNA methylation profiling revealed that the Treg-SE DNA methylation profile of the renewed FOXP3$^+$ population aligned with an nTreg-type profile when compared with direct ex vivo naïve splenic nTregs and iTregs harvested on day 5 of culture (Supplemental Figure 1F).

To generate lineage-identifiable iTregs for adoptive transfer, we first bred mice harboring a tamoxifen-inducible *Foxp3*-Cre driver with a green fluorescent protein (GFP) label (*Foxp3*$^{GFP\text{-}Cre\text{-}ERT2}$) and a *loxP*-flanked stop codon upstream of the red florescent protein, tdTomato, driven by a CAG promoter at the open *ROSA26* locus (*ROSA26Sor*$^{CAG\text{-}tdTomato}$) (30). Then, sorted CD4$^+$ conventional T cells (Tconv, CD4$^+$*Foxp3*-GFP$^-$) from the secondary lymphoid organs of *Foxp3*$^{GFP\text{-}CreERT2}$*Rosa26Sor*$^{CAG\text{-}tdTomato}$ mice were cultured in the presence of T cell receptor stimulation (αCD3ε/αCD28), TGF-β, IL-2, and tamoxifen to induce FOXP3$^+$ cell-specific GFP and tdTomato expression (Supplemental Figure 2A). Separately, CD4$^+$ conventional T cells derived from the same mice were cultured in the presence of T cell receptor stimulation and IL-2, to serve as controls (Supplemental Figure 2A). iTregs and Tconv cells were harvested for adoptive transfer on day 5 of cell culture. Natural Tregs were adoptively transferred directly following isolation from the spleen and lymph nodes of *Foxp3*$^{GFP\text{-}CreERT2}$*Rosa26Sor*$^{CAG\text{-}tdTomato}$ mice (Supplemental Figure 2B). Concurrently, recipient *Foxp3*$^{GFP\text{-}DTR}$ mice received DTx followed by intratracheal instillation with a titer of influenza A virus sufficient to cause 10–20% mortality in Treg-depleted animals. At 5 DPI, 1x10^6 iTregs, nTregs, or Tconv cells or PBS were administered via retroorbital injection (Figure 1A). Although arterial oxyhemoglobin saturation (SpO_2) was similar between groups, mice that received influenza but no DTx (positive control), nTregs (positive control), or iTregs experienced significantly greater survival compared with mice that received Tconv cells (negative control) or PBS (vehicle control) (Figure 1, B and C). Mice that received influenza but no DTx displayed a more rapid recovery in mass as well as a significantly lower absolute number of lung-infiltrating leukocytes compared with the other groups (Supplemental Figure 2, C and D). Flow cytometric analysis of lung single-cell suspensions at 24 DPI revealed a greater percentage of alveolar epithelial cells, including alveolar epithelial type 2 (ATII) cells (CD326$^+$MHCII$^+$T1A$^-$/CD326$^+$CD31$^-$CD45$^-$) (40), in mice that received nTregs or no DTx compared with mice that received Tconv or PBS (Figure 1, D and E). Unexpectedly, mice that received iTregs displayed the lowest percentage of ATII cells among the experimental groups. To further characterize the effect of iTreg adoptive transfer on epithelial repair, we examined the KRT5$^+$ epithelial cell population, a marker of dysregulated and incomplete repair (41-43). Mice that received iTregs displayed the lowest percentage of KRT5$^+$ epithelial cells, suggesting effective repair despite the reduced percentage of ATII cells (Figure 1F). We observed no significant differences in the frequency of proliferating (Ki-67$^+$) ATII cells between groups that received DTx (Figure 1G) or in absolute epithelial or endothelial cell numbers between groups (Supplemental Figure 2, E-I). To define and assess transcriptional signature differences between nTregs and iTregs after influenza

infection, we compared iTregs harvested from lungs 24 DPI to a previously defined gene cluster associated with repair function in nTregs harvested from the lungs of 8–12 week-old *Foxp3*$^{GFP\text{-}DTR}$ mice at a late repair time point (40). We found a high degree of similarity in gene expression between lung iTregs and nTregs during repair; this gene set included several genes known to be associated with Treg repair function (*Bmper, Ereg, Fgf1, Hhip, Hoxa5, Igf1, Lama3, Lox, Mmp12,* and *Pdgfa*) (Supplemental Figure 3A and Supplemental Table 1). Taken together, these results suggest iTreg adoptive transfer is beneficial to alveolar epithelial repair.

UHRF1 is dispensable for iTreg FOXP3 induction and stability but is required to maintain transcriptional and epigenetic programs in vitro.

To test whether UHRF1-mediated maintenance DNA methylation is necessary for iTreg differentiation and stability in vitro, we first bred *Uhrf1*$^{fl/fl}$*Foxp3*$^{GFP\text{-}CreERT2}$*Rosa26Sor*$^{CAG\text{-}tdTomato}$ mice (referred to here as *Uhrf1*$^{fl/fl}$). This gene combination results in inducible, Treg-specific, *Foxp3* lineage-traceable iTregs that lose UHRF1 expression contemporaneously with FOXP3 induction (30). CD4$^+$*Foxp3*-GFP$^+$ cells (nTregs) and CD4$^+$*Foxp3*-GFP$^-$ T cells were isolated from the spleens of *Uhrf1*$^{+/+}$ (control) or *Uhrf1*$^{fl/fl}$ mice. Natural Tregs were cultured in the presence of αCD3ε/αCD28 activation beads at a ratio of three beads to one Treg cell and recombinant human IL-2 at a concentration of 2,000 U/ml. CD4$^+$*Foxp3*-GFP$^-$ T cells were cultured in αCD3ε/αCD28 coated plates, recombinant human IL-2 (50 U/ml), and TGF-β (10ng/ml) (Figure 2A). From each genotype, one group of nTregs and iTregs was treated with tamoxifen during the initial 5 days of culture (denoted as the "early" group). Cells from this early culture were harvested and sorted for bulk RNA-seq analysis on day 5 or cultured for an additional 7 days without tamoxifen then sorted for bulk RNA-seq analysis on culture day 12 (Figure 2A)**.** A separate group of nTregs and iTregs that was not exposed to tamoxifen during the first 5 days of culture (denoted as the "delayed" group) was either sorted for bulk RNA-seq on culture day 5 or transitioned into media with tamoxifen and cultured for an additional 7 days before sorting for RNA-seq analysis on culture day 12. Consistent with published data (30,31), flow cytometry analysis demonstrated no significant difference in FOXP3 induction or stability in iTregs (i.e., ex-FOXP3 cells) over the culture period regardless of when UHRF1 was deleted (Figure 2B). We confirmed that CD4$^+$*Foxp3*-GFP$^+$ iTregs and nTregs from *Uhrf1*$^{+/+}$ mice sorted on day 5 of cell culture expressed high levels of canonical Treg signature genes (e.g.,

Il2ra, *Il2rb*, *Icos*, *Tigit*, *Il10*, *Gzmb*, *Ctla4*, *Nt5e*, *Itgae*, *Nrp1*, and *Lag3*) (Supplemental Figure 3, B and C). We additionally confirmed the in vitro suppressive function of iTregs following 5 days of culture, finding no significant difference between *Uhrf1*$^{+/+}$ and *Uhrf1*$^{fl/fl}$ cells (Figure 2C). Principal component analysis (PCA) of 6,978 differentially expressed genes (DEGs) identified from ANOVA-like testing with FDR $q < 0.05$ in "early" and "delayed" groups of *Uhrf1*$^{+/+}$ and *Uhrf1*$^{fl/fl}$ nTregs and iTregs at days 5 and 12 of culture demonstrated clustering by cell culture condition and cell type. PC1 reflected the transcriptional differences between nTregs and iTregs; PC2 reflected time in culture (day 5 versus day 12) (Figure 2D). Notably, transcriptional differences in nTregs as a function of when UHRF1 was deleted were minimal, as clustering remained tight regardless of time in culture and timing of UHRF1 loss. The loss of UHRF1 concurrent with FOXP3 induction (early) in iTregs had a nominal effect (≤3 DEGs) on the iTreg transcriptome when compared with *Uhrf1*$^{+/+}$ iTregs. Nevertheless, within PC2, we noted sub-clustering within iTregs on day 12 of culture that reflected the time when UHRF1 was deleted after FOXP3 induction. Pairwise comparison of *Uhrf1*$^{+/+}$ and *Uhrf1*$^{fl/fl}$ cells from the delayed group analyzed on day 12 revealed 127 DEGs, with genes upregulated in *Uhrf1*$^{+/+}$ iTregs including those associated with chemotaxis and migration (*Ccr5*, *Ccr8*, and *S1pr2*) as well as Treg proliferation, differentiation, and transcriptional stabilization (*Skp2*, *Lif*, and *Dusp4*) (Figure 2, E and F, and Supplemental Table 1). Gene set enrichment analysis (GSEA) comparing these iTregs revealed positive enrichment of genes in the *Uhrf1*$^{+/+}$ iTregs previously annotated to be upregulated in nTregs and iTregs compared with CD4$^+$ Tconv cells in a similar *Foxp3*-GFP IRES construct mouse model as well as an alternate *Foxp3*-GFP chimeric fusion model in which the GFP coding region is inserted in-frame into the N-terminal domain of the *Foxp3* locus, resulting in divergent immunoregulatory functions (Figure 2G) (44-46). This analysis also revealed positive enrichment of genes in *Uhrf1*$^{+/+}$ iTregs previously annotated to be upregulated following successful induction of FOXP3 compared with CD4$^+$ Tconv cells from the same culture that failed to express FOXP3 (44). *Uhrf1*$^{fl/fl}$ iTregs were positively enriched in genes previously annotated to be downregulated in iTregs compared with CD4$^+$ Tconv cells (44). Additional GSEA demonstrated positive enrichment of hallmark processes associated with Treg function in *Uhrf1*$^{+/+}$ cells, including Myc targets, E2F targets, TGF-β signaling, WntB catenin signaling, TNF-α signaling via NFκB, MTORC signaling, KRAS signaling, and IL-2–STAT5 signaling (Supplemental Figure 3D and Supplemental Table 2). No hallmark gene sets were significantly positively enriched in *Uhrf1*$^{fl/fl}$ iTregs. To confirm that maintenance DNA methylation was lost upon UHRF1 deletion, we performed genome-wide 5′-cytosine–phosphate–guanine-3′ (CpG) methylation profiling with modified reduced representation

bisulfite sequencing of *Uhrf1*$^{+/+}$ and *Uhrf1*$^{fl/fl}$ iTregs from both the "early" and "delayed" groups at day 12 of culture. PCA of approximately 80,000 differentially methylated cytosines (FDR $q < 0.05$) revealed distinct clustering according to culture condition (Figure 2H). PC1 reflected methylation changes based on the deletion of UHRF1, whereas PC2 reflected methylation changes based on the timing of UHRF1 deletion. Pairwise comparison of *Uhrf1*$^{+/+}$ and *Uhrf1*$^{fl/fl}$ iTregs in the delayed group at day 12 demonstrated hypomethylation in *Uhrf1*$^{fl/fl}$ iTregs (Figure 2I). Taken together, these results indicate that UHRF1-mediated maintenance DNA methylation is dispensable for the establishment of iTreg FOXP3 expression, transcriptional identity, and suppressive function but is necessary for the subsequent stability of the iTreg transcriptomic signature in vitro.

UHRF1-deficient iTregs fail to promote recovery following viral pneumonia.

Because the loss of UHRF1-mediated maintenance DNA methylation promoted transcriptional instability in iTregs, we asked whether the loss of UHRF1 limits the ability of adoptively transferred iTregs to promote recovery following influenza pneumonia. Using the data generated from recipients of UHRF1-sufficient iTregs *(Uhrf1*$^{+/+}$) as a control (presented in Figure 1, B-G) and generated in contemporaneous experiments as the data generated from mice which received UHRF1-deficient mice (*Uhrf1*$^{fl/fl}$) to perform a zoomed-in comparison with recipients of *Uhrf1*$^{fl/fl}$ iTregs, we found that mice that received UHRF1-deficient (*Uhrf1*$^{fl/fl}$) iTregs experienced worsened mortality and hypoxemia compared with mice that received *Uhrf1*$^{+/+}$ iTregs (Figure 3, A and B). We observed no significant differences in mass recovery (Supplemental Figure 4). Flow cytometry analysis of post-caval lobe single-cell suspensions at 24 DPI revealed a greater frequency and total number of alveolar epithelial cells and alveolar epithelial type 2 (ATII) cells in *Uhrf1*$^{fl/fl}$ iTreg recipients compared with *Uhrf1*$^{+/+}$ iTreg recipients (Figure 3, C-F). Notably, compared with recipients of *Uhrf1*$^{+/+}$ iTregs, *Uhrf1*$^{fl/fl}$ iTreg recipients also displayed a greater frequency and total number of KRT5^{+} epithelial cells and a higher total number, but not frequency, of Ki-67^{+} ATII cells, suggesting a greater degree of peak injury in the recipients of *Uhrf1*$^{fl/fl}$ iTregs (Figure 3, G-J). Collectively, adoptive transfer of UHRF1-deficient iTregs compromised recovery from viral pneumonia and recipients of *Uhrf1*$^{fl/fl}$ iTregs displayed evidence of a greater degree of peak injury.

Adoptive transfer of UHRF1-deficient iTregs results in delayed repair of lung injury following viral pneumonia compared with UHRF1-sufficient iTregs

In addition to promoting repair, Tregs possess distinct tissue-protective properties that impart resilience to damage (47). As analysis of our adoptive transfer experiments at a late repair timepoint (24 DPI) demonstrated a reduced frequency of ATII cells in recipients of *Uhrf1*$^{+/+}$ iTregs compared with recipients of *Uhrf1*$^{fl/fl}$ iTregs despite reduced hypoxemia and mortality, we hypothesized that *Uhrf1*$^{+/+}$ iTregs impart resilience to lung injury by decreasing infiltration by inflammatory immune cells or by dampening early injury to result in a less robust repair response later in the disease course. We therefore performed an additional series of adoptive transfer experiments with analysis at 11 DPI, a timepoint that correlated with peak lung injury. Like experiments analyzed on 24 DPI, *Uhrf1*$^{+/+}$ and *Uhrf1*$^{fl/fl}$ iTregs were treated with tamoxifen for 3 days and cells were harvested for adoptive transfer on culture day 5. We found no difference in immune cell infiltration, including total leukocytes and myeloid and lymphoid cell subsets (Supplemental Figure 5, A-F). In contrast, lungs from mice that received *Uhrf1*$^{+/+}$ iTregs displayed a significantly greater total number of ATII cells with a concomitantly greater total number of Ki-67^{+} ATII cells compared with recipients of *Uhrf1*$^{fl/fl}$ iTregs (Figure 4, A and B). No significant differences were observed in total numbers of epithelial or KRT5^{+} epithelial cells (Supplemental Figure 5, G and H). Interestingly, recipients of *Uhrf1*$^{fl/fl}$ iTregs displayed a significantly greater total number of endothelial cells when directly compared with recipients of *Uhrf1*$^{+/+}$ iTregs (Figure 4C). We quantified the adoptively transferred tdTomato^{+} iTregs and found a significantly lower frequency and total number of *Uhrf1*$^{fl/fl}$ iTregs in the lungs compared with *Uhrf1*$^{+/+}$ iTregs (Figure 4, D-E). No significant difference was observed in the frequency of ex-FOXP3 cells between groups (Figure 4F). To assess whether the inflammatory microenvironment of the lung could be influencing the differences in engraftment following adoptive transfer, we quantified tdTomato^{+} iTregs from the spleens of these mice and found that the frequency but not total number of iTregs was lower in recipients of *Uhrf1*$^{fl/fl}$ compared with *Uhrf1*$^{+/+}$ iTregs (Figure 4, G and H). Consistent with data from the lungs, no difference was observed in the frequency of ex-FOXP3 cells in the spleen (Figure 4I). Taken together with the data from 24 DPI, these results suggest that UHRF1-deficient iTregs provide an insufficient early tissue-protective response that results in delayed repair.

To differentiate between an intrinsic difference in functionality of *Uhrf1*$^{fl/fl}$ iTregs versus dysfunctionality due to their diminished engraftment, we performed an additional adoptive transfer experiment in which we attempted to equalize the number of engrafted cells. Based on differences we observed in the total number and frequency of cells between *Uhrf1*$^{+/+}$ and *Uhrf1*$^{fl/fl}$ iTregs in the lungs at 11 DPI, we estimated that adoptive transfer of 4x10^6 *Uhrf1*$^{fl/fl}$ iTregs would be sufficient. Mice that received 1x10^6 *Uhrf1*$^{+/+}$ iTregs or 1x10^6 *Uhrf1*$^{fl/fl}$ iTregs served as positive and negative controls, respectively. Intriguingly, and consistent with prior experiments, mice that received 1x10^6 *Uhrf1*$^{+/+}$ iTregs exhibited significantly greater SpO_2 compared with mice that received either quantity of *Uhrf1*$^{fl/fl}$ iTregs (Supplemental Figure 6A). Recipients of 1x10^6 *Uhrf1*$^{+/+}$ iTregs exhibited a trend toward greater survival (Supplemental Figure 6B). Mice that received 1x10^6 *Uhrf1*$^{+/+}$ iTregs also exhibited reduced mass loss over the course of influenza (Supplemental Figure 6C). Despite the 4-fold difference in adoptively transferred *Uhrf1*$^{fl/fl}$ iTregs, quantification of adoptively transferred iTregs in the lungs and spleens of influenza-infected mice at 24 DPI revealed a significantly lower frequency and total number of *Uhrf1*$^{fl/fl}$ iTregs and, unlike at 11 DPI, a concomitantly larger *Foxp3*-GFP$^-$tdTomato$^+$ ex-FOXP3 population in recipients of *Uhrf1*$^{fl/fl}$ iTregs (Supplemental Figure 6, D-I). Nevertheless, the quantity of *Uhrf1*$^{fl/fl}$ iTregs in recipients of 4x10^6 *Uhrf1*$^{fl/fl}$ iTregs was significantly higher than in recipients of 1x10^6 *Uhrf1*$^{fl/fl}$ iTregs. Taken together, the inability to equalize the number of engrafted iTregs in a linear fashion by administering a higher adoptive transfer dose further supports a substantial defect in recruitment attributable to the loss of UHRF1.

UHRF1-deficient iTregs display transcriptional instability and poor engraftment after adoptive transfer into mice with viral pneumonia.

To explore cell-intrinsic mechanisms underlying the loss of pro-recovery function in UHRF1-deficient iTregs, we profiled *Foxp3*-GFP$^+$tdTomato$^+$ iTregs sorted from the lungs of *Uhrf1*$^{+/+}$ and *Uhrf1*$^{fl/fl}$ iTreg recipients at 24 DPI. The frequency of adoptively transferred cells that had lost FOXP3 expression (*Foxp3*-GFP$^-$TdTomato$^+$; ex-FOXP3 cells) was not significantly different between *Uhrf1*$^{+/+}$ and *Uhrf1*$^{fl/fl}$ iTregs though the trend reflects a larger ex-FOXP3 population in *Uhrf1*$^{fl/fl}$ iTregs as seen in the data presented in Supplemental Figure 6 (Figure 5A). Looking beyond stability at the FOXP3 locus, we subsequently focused our analysis on transcriptomic comparison of *Uhrf1*$^{+/+}$ and *Uhrf1*$^{fl/fl}$ iTregs. We identified 1,187 DEGs;

k-means clustering of these DEGs identified two distinct clusters (Figure 5B and Supplemental Table 1). Genes upregulated in *Uhrf1*$^{+/+}$ iTregs included several associated with Treg pro-repair function or tissue repair, such as *Notch4*, *Dll4*, *Pdgfra*, *Mmp12*, *Fgfr1*, *Loxl2*, *Wnt8b*, and *Yap1* (Figure 5C). In contrast, several genes upregulated in *Uhrf1*$^{fl/fl}$ iTregs are associated with effector helper T cell lineage commitment, such as *Stat3*, *Il6ra*, *Jak1*, *Itk*, *Igfbp4*, *Zeb1*, *Gata3*, *Il4ra*, and *Ifnar1*. GSEA revealed positive enrichment of genes sets associated with IL-6–STAT3 signaling as well as negative enrichment of genes associated with angiogenesis and epithelial to mesenchymal transition in *Uhrf1*$^{fl/fl}$ iTregs (Figure 5, D and E and Supplemental Table 3). Functional enrichment analysis revealed upregulation of gene sets associated with protein translation, interferon and interleukin signaling, helper T cell and Th17 differentiation, viral processes, DNA damage repair, cellular stress responses, and apoptotic processes in *Uhrf1*$^{fl/fl}$ iTregs (Figure 5F and Supplemental Table 3). We quantified the number of transferred iTregs in the lungs of recipient mice at 24 DPI and again found a significantly reduced frequency and total number of *Uhrf1*$^{fl/fl}$ iTregs compared with *Uhrf1*$^{+/+}$ iTregs (Figure 5, G and H).

To assess for extra-pulmonary signatures due to the loss of UHRF1, we sorted *Foxp3*-GFP^{+}tdTomato^{+} and *Foxp3*-GFP^{-} tdTomato^{+} (ex-FOXP3) cells from the spleens of *Uhrf1*$^{+/+}$ and *Uhrf1*$^{fl/fl}$ iTreg recipients at 24 DPI for gene expression profiling. PCA of 457 differentially expressed genes identified following ANOVA-like testing with FDR $q < 0.05$ demonstrated clustering by genotype and FOXP3 expression (Supplemental Figure 7A). PC1 reflected the transcriptional differences dependent on FOXP3 expression, and PC2 reflected differences between genotype (*Uhrf1*$^{+/+}$ versus *Uhrf1*$^{fl/fl}$). Pairwise comparison of *Uhrf1*$^{+/+}$ and *Uhrf1*$^{fl/fl}$ FOXP3^{+} cells revealed 183 DEGs, with genes upregulated in *Uhrf1*$^{+/+}$ iTregs associated with cell cycle regulation/cellular proliferation and induction and maintenance of Treg function (*E2f3*, *Ncoa3*, *Hpse*) (Supplemental Figure 7, B and C and Supplemental Table 1). Genes upregulated in *Uhrf1*$^{fl/fl}$ iTregs included those associated with maintenance of function but also proinflammatory cytokines and cytokine receptors (*Mst1*, *Tmed4, Il1b*, *Il17rb*, and *Il4*). Pairwise comparison of *Uhrf1*$^{+/+}$ and *Uhrf1*$^{fl/fl}$ ex-FOXP3 cells revealed 274 DEGs, with genes upregulated in *Uhrf1*$^{+/+}$ ex-FOPX3 cells associated with Treg stability and suppressive function (*Ikzf2, Zap70, Tnfrsf9, Il1r1,* and *Parp11*). Genes upregulated in *Uhrf1*$^{fl/fl}$ ex-FOXP3 cells included some associated with alternate effector T cell function and apoptosis (*Il17rb, Il13, Crtc2, Casp8ap2,* and *Tnfrs8*) (Supplemental Figure 7, D and E and Supplemental Table 1).

To further elucidate whether engraftment was influenced by the inflammatory microenvironment of the lung, we harvested adoptively transferred *Foxp3*-GFP^{+}tdTomato^{+} cells from the spleens and lungs of *Foxp3*$^{GFP\text{-}DTR}$ recipients of *Uhrf1*$^{+/+}$ or *Uhrf1*$^{fl/fl}$ iTregs that received DTx but not influenza. We found that iTregs in recipients of *Uhrf1*$^{+/+}$ iTregs were consistently greater in frequency and total number compared with recipients of *Uhrf1*$^{fl/fl}$ iTregs and intriguingly displayed a significantly greater degree of instability (ex-FOXP3 cells) in the lungs but not the spleen (Supplemental Figure 8, A-G). Collectively, these data suggest that iTregs require UHRF1 to stabilize their phenotypic identity, upregulate repair processes, and promote tissue engraftment following influenza virus pneumonia.

Loss of UHRF1-mediated maintenance DNA methylation results in disrupted DNA methylation and delayed expression of signature Treg transcriptional programs.

To determine transcriptional differences in iTregs earlier in the course of injury and assess for differences in the transcriptional landscape over time, we compared transcriptional profiling of sorted *Foxp3*-GFP^{+}tdTomato^{+} cells from the lungs on 11 and 24 DPI from DTx treated, influenza-infected mice that received adoptive transfer of *Uhrf1*$^{fl/fl}$ or *Uhrf1*$^{+/+}$ iTregs on 5 DPI. PCA of 2,117 DEGs identified following ANOVA-like testing with FDR $q < 0.05$ demonstrated clustering by DPI and genotype (Figure 6A). PC1 reflected the transcriptional differences between iTregs at 11 versus 24 DPI, and PC2 reflected differences between genotypes (*Uhrf1*$^{+/+}$ versus *Uhrf1*$^{fl/fl}$) at 24 DPI. Pairwise comparison of *Foxp3*-GFP^{+}tdTomato^{+} cells isolated at 11 DPI revealed 32 DEGs. GSEA revealed positive enrichment of hallmark processes associated with essential Treg functions, including Myc targets, oxidative phosphorylation, E2F targets, TNF-α signaling via NFκB, MTORC signaling, and IL-2–STAT5 signaling in *Uhrf1*$^{+/+}$ iTregs. No processes were positively enriched in *Uhrf1*$^{fl/fl}$ iTregs on 11 DPI (Figure 6B and Supplemental Table 4). Additional GSEA revealed a similar pattern, with positive enrichment of GO processes seen in *Uhrf1*$^{+/+}$ iTregs including protein translation, T cell differentiation, regulation of lymphocyte-mediated immunity, DNA damage repair, cellular stress responses, and apoptotic processes, but no positively enriched processes in *Uhrf1*$^{fl/fl}$ iTregs (Figure 6C and Supplemental Table 4). An unsupervised analysis comparing differentially methylated regions (DMRs) of *Uhrf1*$^{fl/fl}$ and *Uhrf1*$^{+/+}$ iTregs at 24 DPI with at least a 10% difference in methylation demonstrated disrupted methylation at 34 regions in *Uhrf1*$^{fl/fl}$ iTregs (Figure 6D and Supplemental Table 1).

These findings fit a pattern in which processes enriched in *Uhrf1*$^{+/+}$ iTregs at 11 DPI are not enriched in *Uhrf1*$^{fl/fl}$ iTregs until 24 DPI, suggesting a delayed transcriptomic phenotype paralleling the delayed repair phenotype of the recipient mice.

Discussion

Natural Tregs depend on specific patterns of DNA methylation to establish cell identity and stability as well as to exert their pro-recovery function following acute lung injury (8,12,30,48). Here, we demonstrated the ability of transferred iTregs to promote recovery following viral pneumonia in mice. We further demonstrated that maintenance DNA methylation mediated by the epigenetic regulator, UHRF1, is necessary for iTreg reparative function during viral pneumonia. Recipients of UHRF1-deficient iTregs experienced worsened hypoxemia and mortality with dysregulated and delayed lung repair. In vitro, the loss of maintenance DNA methylation resulted in downregulation of chemokine receptor gene expression, such as *Ccr4*, *Ccr5*, and *Ccr8*. In vivo, UHRF1-deficient iTregs displayed reduced lung tissue engraftment, greater propensity for instability in FOXP3 expression, and downregulation of genes associated with pro-repair function and upregulation of pro-apoptotic genes and alternate effector T cell lineage defining transcription factors. These findings support the use of iTregs for cellular therapy while demonstrating the necessity of maintenance DNA methylation in iTreg stability and function.

Our observations support a paradigm in which critical changes occur across the DNA methylation landscape between the $CD4^+$ stage of T cell development and subsequent FOXP3 expression that cause a differential effect of the loss of maintenance DNA methylation on iTreg function. We demonstrated that iTregs that lose UHRF1 following FOXP3 induction possess a reduced ability to protect the lung from alveolar epithelial injury, leading to delayed lung repair. In contrast, other studies demonstrate that iTregs generated from UHRF1-deficient $CD4^+$ T cells exhibit hyper-suppressive function when adoptively transferred into lymphocyte-deficient mice with Tconv cell-mediated colitis (31). In both cases, the loss of UHRF1 did not affect FOXP3 induction, yet, here, the loss of UHRF1 resulted in greater instability in vivo while also altering the transcriptome at other loci. A similar effect dependent on the timing of loss of UHRF1 exists in nTregs (30,49). Indeed, work from our group demonstrated that the loss of UHRF1 at the $FOXP3^+$ stage of nTreg development caused the spontaneous onset of widespread scurfy-like inflammation (30). Intriguingly, in that study, we also observed the generation of ex-FOXP3 cells following the induced loss of UHRF1 in vivo, suggesting a link between UHRF1-mediated maintenance DNA methylation and the stability of FOXP3 expression in Tregs. In contrast, mice with pan-T cell UHRF1 deficiency develop inflammation localized specifically to the colon (49). Although the latter study noted differences in

thymic and peripheral Treg populations, it further serves as evidence of the differential effect of the loss of UHRF1 depending on the developmental stage of the Treg.

Despite reports of instability of iTregs within inflammatory microenvironments, our data suggest that iTregs retain their function in promoting lung repair, like adoptively transferred nTregs (12,16-18). Suppressive mechanisms did not appear to play a role in the differential effects of the loss of UHRF1, as immune infiltration and activation were similar in mice that received UHRF1-sufficient and -deficient iTregs. Whether and how the inflammatory microenvironment contributed to reduced engraftment of UHRF1-deficient iTregs is unclear. RNA sequencing data from cells cultured in vitro suggest that reduced engraftment may be a result of lower homing receptor expression, such as CCR4, 5, and 8. In addition, data from UHRF1-deficient iTregs recovered from the lung revealed upregulation of several pro-apoptotic factors, suggesting an influence from the inflammatory microenvironment that reduced UHRF1-deficient iTreg numbers.

iTregs may therefore serve as a practical, safe, and efficient alternative to nTreg cellular therapy for severe, rapidly progressive, tissue-injurious inflammatory diseases, such as ARDS (50). Currently, nTregs are obtained via leukapheresis from autologous peripheral or allogeneic cord blood, and protocols to expand them are on the order of weeks (51,52). This same process could be applied to iTregs in a fraction of the time, as they derive from $CD4^+$ Tconv cells and expand rapidly in culture, allowing for intervention at an earlier time point in the disease course. Similar to strategies for nTregs, ex vivo modification strategies could be implemented to further enhance iTreg therapeutic efficacy (15). As we noted cellular engraftment may play a role in the differential effects observed in recipients of UHRF1-sufficient and -deficient iTregs, in vitro supplementation with factors to promote homing to the site of injury via enhanced chemokine receptor expression could ensure arrival of the transferred cell product to the site of injury. Additionally, because the loss of UHRF1-mediated maintenance DNA methylation resulted in upregulation of genes associated with effector helper T cell lineage commitment, factors to promote their downregulation could be leveraged to ensure stable functioning.

In summary, our data establish that iTregs promote timely repair of damaged lung tissue following viral pneumonia. Mechanistically, UHRF1-mediated maintenance DNA methylation is required for optimal iTreg engraftment and reparative function. These data credential iTregs as potential cellular therapy to promote repair following viral pneumonia-induced acute lung injury.

Methods

Sex as a biological variable

In preliminary experiments using the influenza model in wild-type mice, we found that female mice experienced higher mortality than males. As recipients of *Uhrf1*$^{fl/fl}$ iTregs experienced higher mortality than controls, male mice were used for these experiments. Hence, sex was not considered as a biological variable in all experiments.

Mice

All mice were housed and used in accordance with the Institutional Animal Care and Use Committee (IACUC) at Northwestern University. Animals received water ad libitum, were housed at a temperature range of 20 °C to 23 °C under 14-hour light/10-hour dark cycles and received standard rodent chow. For all experiments male mice between 8 and 20 weeks of age were used. *Foxp3*$^{GFP\text{-}DTR}$ mice were purchased from The Jackson Laboratory (strain no. 016958) and bred on-site. *Foxp3*^{Cre} mice were purchased from the Jackson Laboratory (strain no. 016959) and bred on-site. C57BL/6 *Uhrf1*$^{fl/fl}$*Foxp3*$^{GFP\text{-}CreERT2}$*Rosa26Sor*$^{CAG\text{-}tdTomato}$ or *Foxp3*$^{GFP\text{-}CreERT2}$*Rosa26Sor*$^{CAG\text{-}tdTomato}$ mice were generated as previously described (30). All animals were genotyped using services provided by Transnetyx Inc., with primer sequences provided by The Jackson Laboratory or published in prior work (30).

Diphtheria toxin, influenza A virus administration, and adoptive transfer

To ablate the endogenous mouse Treg population, lyophilized diphtheria toxin (List Biological Laboratories, product no. 150) was resuspended in sterile PBS and administered in 100 µl via intraperitoneal injection every two days to *Foxp3*$^{GFP\text{-}DTR}$ mice. The initial loading dose was 50 µg/kg followed by maintenance dosing of 10 µg/kg. For influenza A virus administration, mice were intubated while under isoflurane anesthesia using a 20-gauge angiocatheter cut to a length that placed the tip of the catheter above the carina. Following intubation, a 1ml syringe containing 50ul of sterile PBS and with the plunger removed was attached onto the angiocatheter to act as a spirometer and confirm proper placement into

the trachea. Once proper placement was confirmed, the mice were then instilled with mouse-adapted influenza A/WSN/33 H1N1 virus in 50 µL of sterile PBS as previously described (33,40,53-55). A 300ul bolus of air from a second 1ml syringe was ejected into the angiocatheter to clear it and ensure the bolus of influenza was well distributed into the lungs. Natural Tregs were adoptively transferred directly following isolation from the spleen and lymph nodes of 8–12-week-old *Foxp3*$^{GFP\text{-}CreERT2}$*Rosa26Sor*$^{CAG\text{-}tdTomato}$ mice using the mouse Miltenyi CD4$^+$CD25$^+$ Regulatory T Cell Isolation Kit (cat. no. 130-091-041). For conventional T cell and iTreg adoptive transfer, cells were harvested from culture on day 5, re-stained for CD4 and viability dye, and sorted via a microfluidics MACSQuant® Tyto® sorter (Miltenyi) to enhance purity (Supplemental Table 5). Cells were subsequently washed twice and resuspended in sterile PBS at a concentration of 1x10^6 cells/100 µl. Once resuspended, cells were drawn up into a 500-µl insulin syringe (BD ref 329461) and delivered into mice placed under isoflurane anesthesia via the retroorbital sinus (40).

Cell culture and preparation for adoptive transfers

To prepare conventional T cells and iTregs for cell culture prior to adoptive transfer, spleens and lymph nodes (inguinal and axillary) were harvested from adult (8–12-week-old) mice and disrupted using scored 60-mm petri dishes in PBS and filtered through a 40-µm nylon mesh filter to obtain single-cell suspensions. Red blood cell lysis was performed using Gibco ACK lysing buffer (cat. no. A1049201). Cell counts were obtained using a Cellometer K2 Counter using AOPI stain (Nexcelom Bioscience cat. no. SD014-0106). CD4$^+$ T cells were purified from single-cell suspension using the EasySep™ mouse CD4$^+$ T cell Isolation Kit (Stemcell, cat. no. 19852) or the negative fraction of the Miltenyi mouse CD4$^+$CD25$^+$ Regulatory T cell Isolation Kit (cat. no. 130-091-041) according to the manufacturer's instructions. To further enhance purity prior to culture, enriched CD4$^+$ single-cell suspensions were stained with antibodies against CD4 for flow cytometry sorting (Supplemental Table 5). Conventional CD4$^+$ T cells were separated from CD4$^+$*Foxp3*-GFP$^+$ nTregs with a microfluidics MACSQuant® Tyto® sorter (Miltenyi). Dead cells were excluded using a viability dye for analysis and sorting (Supplemental Table 5) in all experiments. For conventional T cell and iTreg cell culture, 300,000 sorted CD4$^+$*Foxp3*-GFP$^-$ conventional T cells were seeded in 24-well plates (Fisher ref FB012929) coated with αCD3ε/αCD28 antibody (BD Pharmingen cat. no. 553058 and 553295) at concentrations of 3 µg/ml and 5 µg/ml, respectively. Recombinant human

IL-2 was added to the conventional T cell culture at 50 U/ml. To generate iTregs, recombinant human IL-2 and TGF-β (PeproTech cat. no. 100-21-10UG) were added at 50 U/ml and 10 ng/ml, respectively. All cell types were cultured in RPMI 1640 (Gibco cat. no. 11875-093) media supplemented with 10% fetal bovine serum, 5 mM HEPES (Gibco cat. no. 15630080), 100 U/ml penicillin-streptomycin (Gibco cat. no. 15140122), 1 mM Na-pyruvate (Gibco cat. no. 11360-070), 100 mM MEM non-essential amino acids (Gibco cat. no. 11140050), 2 mM L-glutamine (Gibco cat no. 25030081), and 50 µM 2-mercaptoethanol (Sigma-Aldrich cat. no. M3148). For FOXP3$^+$ cell lineage tracing and *Foxp3*-Cre-mediated loss of UHRF1, Z-4-hydroxytamoxifen (Sigma-Aldrich cat. no. H7904) was added to cell culture from day 0 to day 3 at a concentration of 500 nM. Conventional T cells and iTregs were removed from antibody coated plates on day 3 of culture and passaged into fresh, non-coated, plates and additional recombinant human IL-2 and TGF-β were added at 50 U/ml and 10 ng/ml, respectively.

Measurement of physiologic readouts of viral pneumonia progression and recovery

To prepare mice for arterial oxyhemoglobin saturation (SpO_2) measurement, one day prior to influenza inoculation, a depilatory cream containing the active ingredients potassium thioglycolate (4%) and calcium hydroxide (1.5%) (Nair^{TM}) was applied to the hair on the dorsal neck for two minutes and subsequently gently removed with wet gauze under isoflurane anesthesia. A MouseOx Plus pulse oximeter (Starr Life Sciences) was used to measure SpO_2. Unanesthetized mice were immobilized, and an oximeter collar clip was secured to the hairless neck. Baseline SpO_2 and mass measurements were obtained prior to influenza administration with subsequent measurements taken every other day post-inoculation.

Lung tissue harvesting, processing, and analysis

Mice were euthanized using a carbon dioxide euthanasia chamber followed by cervical dislocation and slowly infused with HBSS through the right atrium of the heart to clear the pulmonary circulation of blood. The lungs were then harvested and the larger airways and other mediastinal structures were trimmed. The post-caval lobes were removed and set aside

for epithelial cell analysis by flow cytometry. For adoptively transferred iTreg and infiltrating immune cell analysis, the remaining lung lobes were grossly homogenized with scissors in HBSS containing 2 mg of collagenase D (Sigma Aldrich cat. no. 11088866001) and 0.25 mg of DNAse I (Sigma Aldrich cat. no. 10104159001) per ml. The lung suspensions were subsequently incubated for 45 minutes at 37 °C and then further homogenized using a Miltenyi OctoMACS tissue dissociator using the mouse lung protocol (m_lung_02). For iTreg cell sorting, the single-cell suspension was enriched using a $CD4^+$ antibody (Miltenyi cat. no. 130-101-962) and the lungs were stained using the reagents listed in Supplemental Table 5. A separate aliquot was taken for infiltrating immune cell analysis, which was enriched using $CD45^+$ selection beads (Miltenyi cat. no. 130-052-301) and the cells were stained using the reagents listed in Supplemental Table 5. Mice were included in the final analyses if their lungs displayed evidence of gross injury or they developed desaturation to at least 89%, indicating successful influenza infection.

For post-influenza induced lung injury epithelial repair analysis, the harvested post-caval lobes were injected with 2 mL Dispase (Corning ref. 354325) containing 0.25 mg DNAse I per mL and incubated for 45 minutes at room temperature on a rocker. Afterward, forceps were used to tease apart large pieces of lung tissue followed by more thorough homogenization via vigorous pipetting through wide-bore pipette tips. The homogenized tissue was then incubated for another 10 minutes at room temperature on a rocker and then filtered through 40-µm filters. Following centrifugation, the cells were resuspended in 2 mL ACK RBC lysis buffer and incubated for an additional four minutes at room temperature. The remaining cells were fixed and stained for flow cytometry analysis using the reagents listed in Supplemental Table 5. Data acquisition for analysis was performed using a Symphony A5 instrument with FACSDiva software (BD). Analysis was performed with FlowJo software version 10.

For preparation of lungs for histopathology, mice were euthanized via carbon dioxide euthanasia chamber and a tracheostomy was created. A 20-gauge angiocatheter was subsequently sutured into the trachea via the tracheostomy. The lungs and trachea were removed en bloc and the lungs were inflated to 15 cm H_2O with 4% paraformaldehyde. 5-µm sections from paraffin-embedded lungs were stained with H&E or trichrome and examined using light microscopy with a high-throughput, automated slide imaging system, TissueGnostics (TissueGnostics GmbH). The percentage of damaged lung area as a function of total lung area was determined utilizing the image processing program, Image J.

Tissue preparation, flow cytometry & cell sorting for in vitro RNA-seq analysis

For RNA-seq analysis following in vitro culture, $CD4^+CD25^+$*Foxp3*-GFP^+ Tregs or $CD4^+CD25^-$*Foxp3*-GFP^- T cells were isolated using the mouse Miltenyi $CD4^+CD25^+$ Regulatory T Cell Isolation Kit (cat. no. 130-091-041). For nTreg cell culture, 100,000 $CD4^+CD25^+$*Foxp3*-GFP^+ Tregs were seeded in 96-well round bottom plates (Corning ref. no. 3799) with αCD3ε/αCD28 Dynabeads™ (Gibco ref. no. 11456D) at a ratio of three beads to one nTreg cell and recombinant human IL-2 at a concentration of 2,000 U/ml (NCI Frederick National Laboratory). To generate iTregs, 300,000 $CD4^+CD25^-$*Foxp3*-GFP^- T cells were cultured in αCD3ε/αCD28 coated plates, recombinant human IL-2 (50 U/ml), and TGF-β (10ng/ml). To delete UHRF1 at different times relative to FOXP3 induction, both cell types were cultured in tamoxifen at a concentration of 500nM from day 0-5 of culture ("early" groups) or from day 6-12 of culture ("delayed" groups). On day 5 or 12 of cultures cells were stained with CD4 and viability dye then sorted using a FACSARIA™ 6-Laser Sorter for RNA-seq analysis (Supplemental Table 5).

Suppression assays

For suppression assays, we sorted either direct ex vivo *Uhrf1*$^{+/+}$$CD4^+$*Foxp3*-$GFP^+$ nTregs or *Uhrf1*$^{fl/fl}$ *and Uhrf1*$^{+/+}$$CD4^+$*Foxp3*-$GFP^+$ iTregs from day 5 of early tamoxifen treated cultures (described above), then co-cultured each group at varying ratios with freshly isolated $CD4^+$*Foxp3*-GFP^- conventional T cells labeled with Cell Trace Violet (Invitrogen ref. no. C34557) (40). Treg:$CD4^+$ conventional T cell co-cultures were activated using αCD3ε/αCD28 Dynabead™ particles at a ratio of three beads to one Treg cell. After 72 hours, cells were harvested and analyzed by flow cytometry using a BD LSRFortessa. The division index of each sample was calculated using the proliferation modeling function in FlowJo software version 10. % Suppression = 100-(Division index/Division index of responders alone)*100.

RNA-sequencing and analysis

Adoptively transferred iTregs isolated from the spleen post influenza or from in vitro cultured cells were harvested from splenic single-cell suspension or cell culture, respectively, flow cytometry sorted, and lysed immediately after sorting with QIAGEN RLT Plus (cat. no. 1053393) containing 1% 2-mercaptoethanol. Cells were then subjected to simultaneous RNA and DNA isolation using the QIAGEN AllPrep Micro Kit (cat. no. 80204). RNA-library preparation was performed using the SMARTer Stranded Total RNA-Seq Kit, version 2 (Takara cat. no. 634411) as previously described (30,56,57). Sequencing was performed on an Illumina NextSeq 2000 instrument as previously described (30). For rare adoptively transferred iTregs, cells were flow cytometry sorted following harvest from lung single-cell suspensions and lysed immediately after sorting with 10x RNA lysis buffer containing 5% RNase inhibitor. 50% of the sample was taken for DNA isolation using the QIAGEN AllPrep Micro Kit (cat. no. 80204). RNA-seq libraries were then prepared by using 100 pg total RNA from each sample by following the SMART-Seq v4 Ultra Low Input RNA Kit (Takara Bio user manual). The cDNA was amplified with 11 cycles of PCR. The Nextera XT kit (Nextera XT DNA Library Preparation Kit, Illumina) was used to make cDNA libraries suitable for Illumina sequencing. Prepared libraries were pooled at 4 nM and sequenced on a NextSeq 2000 (Illumina) using 75-base read lengths in single-end mode.

RNA-seq analysis was performed as previously described (53). After sequencing, raw binary base call (BCL) files were converted to FASTQ files using bcl-Convert (version 3.10.5, Illumina). Adaptor trimming, alignment to the GRCm38 reference genome, and quantification were performed using the nf-core/RNA-seq pipeline version 3.9 (implemented in Nextflow 22.04.5 with Northwestern University Genomics Compute Cluster configuration (nextflow run nf- core/rnaseq -profile nu_genomics --genome GRCm38). Differential expression analysis was performed in R package DEseq2 (version 1.38.3 in R 4.2.3). For K means analysis, k was determined using elbow plots and the kmeans function in R stats 3.6.2 (Hartigan–Wong method with 25 random sets and a maximum of 1,000 iterations) was used for clustering. In vitro K means heat maps generated using the Morpheus web interface (https://software.broadinstitute.org/morpheus/). Gene Set Enrichment Analysis was performed using the Broad Institute's GSEA software, version 4.1.0, GSEAPreranked tool (58) with genes ordered by $\log_2$(fold-change) in average expression against the Hallmark gene sets or the Immunologic Signature gene sets housed in the Molecular Signatures Database of the Broad Institute (59).

Modified reduced representation bisulfite sequencing (mRRBS) and reduced representation enzymatic methylation sequencing (RREM-seq) and analysis

mRRBS library preparation for in vitro cultured cells was performed using procedures previously described by our group (30,40,60). Briefly, genomic DNA was isolated from sorted samples via the QIAGEN AllPrep Micro Kit (cat. no. 80204) and quantified with a Qubit 3.0 instrument. Bisulfite conversion was then performed using the EZ DNA Methylation-Lightning Kit (Zymo Research) per the manufacturer's protocol. We next created indexed Illumina-compatible non-directional libraries from bisulfite-converted single-stranded DNA using the Pico Methyl-Seq Library Prep Kit (Zymo Research). Final library size distribution and quality were assessed via high-sensitivity screen tape (TapeStation 4200, Agilent). Libraries were then pooled for sequencing on a NextSeq 2000 (Illumina) instrument using the V2 High Output reagent kit (1 × 75 cycles).

RREM-seq library preparation was performed as previously described (61,62). Briefly, following genomic DNA extraction using the QIAGEN AllPrep DNA/RNA Micro Kit (cat. no. 80204) 0.5–1 ng of genomic DNA was digested using restriction endonuclease MspI (New England Biolabs) and then enzymatically converted with TET2 and APOBEC (New England Biolabs) per the manufacturer's instructions. Random priming, adapter ligation, PCR product clean-up, and final library amplification were performed using the Pico methyl-seq library prep kit (Zymo Research). Unmethylated λ-bacteriophage DNA (1:200 mass ratio; New England Biolabs) was included in all samples to calculate unmethylated cytosine conversion efficiency (on average >99%). Final library size distribution and quality were assessed via high-sensitivity screen tape (TapeStation 4200, Agilent) and sequenced using single-end reads with a NextSeq 2000 (Illumina).

Methylation analysis was conducted as previously described (30,61). Briefly, following sequencing raw binary base call (BCL) files were converted to FASTQ files using bclConvert (version 3.10.5, Illumina) and trimmed using Trim Galore! (version 0.4.3). Bismark (version 0.21.0) was used to perform alignment to the reference genome mm10 (GRCm38) and methylation extraction. Bismark coverage files were used for quantification using SeqMonk (version 1.48.0) and R package DSS (version 2.46.0). Cumulative distribution plots were generated with the ecdf base R function.

Statistics

P-values and *q*-values resulting from two-tailed tests were calculated using statistical tests stated in the figure legends. Statistical analysis was performed using either GraphPad Prism version 10.3.0 or R version 4.2.3. A *p*- or *q*-value of less than 0.05 was considered significant except for GSEA, in which 0.25 was considered significant (58). Outliers were identified and removed via the ROUT method at a Q of 5%. Computational analysis was performed using Genomics Nodes and Analytics Nodes on Quest, Northwestern University's High-Performance Computing Cluster.

Study approval

All animal experiments and procedures were conducted in accordance with the standards established by the US Animal Welfare Act set forth in NIH guidelines and were approved by the IACUC at Northwestern University under protocols IS00012519 and IS00017837.

Data and material availability

The raw sequencing data are available in the GEO repository under accession number GSE290605. Values for all data points in graphs are reported in the Supporting Data Values file.

Author contributions

AMJ, JKG, MATA, SEW, EMS, and BDS contributed to the conception, hypothesis delineation, and design of the study. AMJ, JKG, QL, MATA, KAH, LM-N, NM, CPRF, HAV, EMS, SEW, and BDS performed experiments/data acquisition and analysis. AMJ, EMS, and BDS wrote the manuscript or provided substantial involvement in its revision.

Acknowledgements

AMJ is supported by NIH award F32HL162418. MATA is supported by NIH awards T32GM144295, T32HL076139, and F31HL162490. NM is supported by NIH award T32AI083216. CPRF is supported by T32HL076139. JG is supported by T32HL076139. QL is supported by the David W. Cugell Fellowship and the The Genomics Network (GeNe) Pilot Project Funding. LM-N is supported by the NIH awards K08HL159356, U19AI135964 and the Parker B. Francis Opportunity Award. SEW is supported by the Burroughs Wellcome Fund Career Awards for Medical Scientists. BDS is supported by NIH awards R01HL149883, R01HL153122, P01HL154998, P01AG049665, U19AI135964, and U19AI181102. We wish to acknowledge the Northwestern University Flow Cytometry Core Facility supported by CA060553; the BD FACSAria SORP system was purchased with the support of S10OD011996. We also wish to acknowledge the Northwestern University RNA-Seq Center/Genomics Lab of the Pulmonary and Critical Care Medicine and Rheumatology Divisions. Histology services were provided by the Northwestern University Mouse Histology and Phenotyping Laboratory, which is supported by P30CA060553 awarded to the Robert H. Lurie Comprehensive Cancer Center. This research was supported in part through the computational resources and staff contributions provided by the Genomics Compute Cluster, which is jointly supported by the Feinberg School of Medicine, the Center for Genetic Medicine, and Feinberg's Department of Biochemistry and Molecular Genetics, the Office of the Provost, the Office for Research, and Northwestern Information Technology. The Genomics Compute Cluster is part of Quest, Northwestern University's high performance computing facility, with the purpose to advance research in genomics. The graphical abstract, Figure 1A, Supplemental Figure 1A, and Figure 2A were created using https://www.biorender.com/. "This work is the result of NIH funding, in whole or in part, and is subject to the NIH Public Access Policy. Through acceptance of this federal funding, the NIH has been given a right to make the work publicly available in PubMed Central."

References

1. Sakaguchi S, et al. Immunologic self-tolerance maintained by activated T cells expressing IL-2 receptor alpha-chains (CD25). Breakdown of a single mechanism of self-tolerance causes various autoimmune diseases. *J Immunol.* 1995;155(3):1151-1164.
2. Sakaguchi S, et al. Regulatory T cells and immune tolerance. *Cell.* 2008;133(5):775-787.
3. D'Alessio FR, et al. CD4+CD25+Foxp3+ Tregs resolve experimental lung injury in mice and are present in humans with acute lung injury. *The Journal of Clinical Investigation.* 2009;119(10):2898-2913.
4. Garibaldi BT, et al. Regulatory T cells reduce acute lung injury fibroproliferation by decreasing fibrocyte recruitment. *Am J Respir Cell Mol Biol.* 2013;48(1):35-43.
5. Mock JR, et al. Foxp3+ regulatory T cells promote lung epithelial proliferation. *Mucosal Immunol.* 2014;7(6):1440-1451.
6. Dial CF, et al. Foxp3(+) Regulatory T Cell Expression of Keratinocyte Growth Factor Enhances Lung Epithelial Proliferation. *Am J Respir Cell Mol Biol.* 2017;57(2):162-173.
7. Arpaia N, et al. A Distinct Function of Regulatory T Cells in Tissue Protection. *Cell.* 2015;162(5):1078-1089.
8. Singer BD, et al. Regulatory T cell DNA methyltransferase inhibition accelerates resolution of lung inflammation. *Am J Respir Cell Mol Biol.* 2015;52(5):641-652.
9. Mock JR, et al. Impact of Regulatory T Cells on Type 2 Alveolar Epithelial Cell Transcriptomes during Resolution of Acute Lung Injury and Contributions of IFN-γ. *Am J Respir Cell Mol Biol.* 2020;63(4):464-477.
10. Ma R, et al. Vimentin modulates regulatory T cell receptor-ligand interactions at distal pole complex, leading to dysregulated host response to viral pneumonia. *Cell Rep.* 2024;43(12):115056.
11. Markov NS, et al. Distinctive evolution of alveolar T cell responses is associated with clinical outcomes in unvaccinated patients with SARS-CoV-2 pneumonia. *Nat Immunol.* 2024;25(9):1607-1622.
12. Ohkura N, et al. T cell receptor stimulation-induced epigenetic changes and Foxp3 expression are independent and complementary events required for Treg cell development. *Immunity.* 2012;37(5):785-799.
13. Li X, et al. Function of a Foxp3 cis-element in protecting regulatory T cell identity. *Cell.* 2014;158(4):734-748.

14. Singer BD, Chandel NS. Immunometabolism of pro-repair cells. *J Clin Invest.* 2019;129(7):2597-2607.

15. Joudi AM, et al. Epigenetic Control of Regulatory T Cell Stability and Function: Implications for Translation. *Frontiers in Immunology.* 2022;13.

16. Zhou X, et al. Instability of the transcription factor Foxp3 leads to the generation of pathogenic memory T cells in vivo. *Nature Immunology.* 2009;10(9):1000-1007.

17. Koenecke C, et al. Alloantigen-specific de novo-induced Foxp3+ Treg revert in vivo and do not protect from experimental GVHD. *Eur J Immunol.* 2009;39(11):3091-3096.

18. Schmidt A, et al. Comparative Analysis of Protocols to Induce Human CD4+Foxp3+ Regulatory T Cells by Combinations of IL-2, TGF-beta, Retinoic Acid, Rapamycin and Butyrate. *PLoS One.* 2016;11(2):e0148474.

19. Lal G, et al. Epigenetic regulation of Foxp3 expression in regulatory T cells by DNA methylation. *J Immunol.* 2009;182(1):259-273.

20. Landman S, et al. DNA Methyltransferase Inhibition Promotes Th1 Polarization in Human CD4(+)CD25(high) FOXP3(+) Regulatory T Cells but Does Not Affect Their Suppressive Capacity. *J Immunol Res.* 2018;2018:4973964.

21. Varanasi SK, et al. Azacytidine Treatment Inhibits the Progression of Herpes Stromal Keratitis by Enhancing Regulatory T Cell Function. *J Virol.* 2017;91(7).

22. Someya K, et al. Improvement of Foxp3 stability through CNS2 demethylation by TET enzyme induction and activation. *Int Immunol.* 2017;29(8):365-375.

23. Chan MW, et al. Low-dose 5-aza-2'-deoxycytidine pretreatment inhibits experimental autoimmune encephalomyelitis by induction of regulatory T cells. *Mol Med.* 2014;20(1):248-256.

24. Lu CH, et al. DNA Methyltransferase Inhibitor Promotes Human CD4(+)CD25(h)FOXP3(+) Regulatory T Lymphocyte Induction under Suboptimal TCR Stimulation. *Front Immunol.* 2016;7:488.

25. Han P, et al. Low-dose decitabine modulates T-cell homeostasis and restores immune tolerance in immune thrombocytopenia. *Blood.* 2021;138(8):674-688.

26. Gao CA, et al. Machine learning links unresolving secondary pneumonia to mortality in patients with severe pneumonia, including COVID-19. *J Clin Invest.* 2023;133(12).

27. Bostick M, et al. UHRF1 plays a role in maintaining DNA methylation in mammalian cells. *Science.* 2007;317(5845):1760-1764.

28. Sharif J, et al. The SRA protein Np95 mediates epigenetic inheritance by recruiting Dnmt1 to methylated DNA. *Nature.* 2007;450(7171):908-912.

29. Nishiyama A, et al. Uhrf1-dependent H3K23 ubiquitylation couples maintenance DNA methylation and replication. *Nature.* 2013;502(7470):249-253.

30. Helmin KA, et al. Maintenance DNA methylation is essential for regulatory T cell development and stability of suppressive function. *J Clin Invest.* 2020;130(12):6571-6587.

31. Sun X, et al. TGF-β signaling controls Foxp3 methylation and T reg cell differentiation by modulating Uhrf1 activity. *Journal of Experimental Medicine.* 2019;216(12):2819-2837.

32. Kim JM, et al. Regulatory T cells prevent catastrophic autoimmunity throughout the lifespan of mice. *Nat Immunol.* 2007;8(2):191-197.

33. Mambetsariev N, et al. Regulatory T Cells Require TBET to Regulate Activated CD8+ T Cells During Recovery from Influenza. *American Journal of Respiratory Cell and Molecular Biology.* 2025;72(4):453-456.

34. Wang G, et al. Adipose-tissue Treg cells restrain differentiation of stromal adipocyte precursors to promote insulin sensitivity and metabolic homeostasis. *Immunity.* 2024;57(6):1345-1359.e1345.

35. Yadav M, et al. Neuropilin-1 distinguishes natural and inducible regulatory T cells among regulatory T cell subsets in vivo. *Journal of Experimental Medicine.* 2012;209(10):1713-1722.

36. Soroosh P, et al. Lung-resident tissue macrophages generate Foxp3+ regulatory T cells and promote airway tolerance. *Journal of Experimental Medicine.* 2013;210(4):775-788.

37. Knoechel B, et al. Sequential development of interleukin 2–dependent effector and regulatory T cells in response to endogenous systemic antigen. *Journal of Experimental Medicine.* 2005;202(10):1375-1386.

38. Josefowicz SZ, et al. Extrathymically generated regulatory T cells control mucosal TH2 inflammation. *Nature.* 2012;482(7385):395-399.

39. Gottschalk RA, et al. TCR ligand density and affinity determine peripheral induction of Foxp3 in vivo. *Journal of Experimental Medicine.* 2010;207(8):1701-1711.

40. Morales-Nebreda L, et al. Aging imparts cell-autonomous dysfunction to regulatory T cells during recovery from influenza pneumonia. *JCI Insight.* 2021;6(6).

41. Zuo W, et al. p63(+)Krt5(+) distal airway stem cells are essential for lung regeneration. *Nature.* 2015;517(7536):616-620.

42. Kanegai CM, et al. Persistent Pathology in Influenza-Infected Mouse Lungs. *Am J Respir Cell Mol Biol.* 2016;55(4):613-615.

43. Vaughan AE, et al. Lineage-negative progenitors mobilize to regenerate lung epithelium after major injury. *Nature.* 2015;517(7536):621-625.

44. Haribhai D, et al. A Central Role for Induced Regulatory T Cells in Tolerance Induction in Experimental Colitis1. *The Journal of Immunology.* 2009;182(6):3461-3468.

45. Darce J, et al. An N-Terminal Mutation of the Foxp3 Transcription Factor Alleviates Arthritis but Exacerbates Diabetes. *Immunity.* 2012;36(5):731-741.

46. Hill JA, et al. Retinoic Acid Enhances Foxp3 Induction Indirectly by Relieving Inhibition from CD4+CD44hi Cells. *Immunity.* 2008;29(5):758-770.

47. Jovisic M, et al. Differential roles of regulatory T cells in acute respiratory infections. *J Clin Invest.* 2023;133(14).

48. Michki NS, et al. DNA methyltransferase inhibition induces dynamic gene expression changes in lung CD4(+) T cells of neonatal mice with E. coli pneumonia. *Sci Rep.* 2023;13(1):4283.

49. Obata Y, et al. The epigenetic regulator Uhrf1 facilitates the proliferation and maturation of colonic regulatory T cells. *Nat Immunol.* 2014;15(6):571-579.

50. Gladstone DE, et al. Randomized, double-blinded, placebo-controlled trial of allogeneic cord blood T-regulatory cells for treatment of COVID-19 ARDS. *Blood Adv.* 2023;7(13):3075-3079.

51. Di Ianni M, et al. Immunomagnetic isolation of CD4+CD25+FoxP3+ natural T regulatory lymphocytes for clinical applications. *Clin Exp Immunol.* 2009;156(2):246-253.

52. Fritsche E, et al. Toward an Optimized Process for Clinical Manufacturing of CAR-Treg Cell Therapy. *Trends Biotechnol.* 2020;38(10):1099-1112.

53. Torres Acosta MA, et al. AMPK is necessary for Treg functional adaptation to microenvironmental stress during malignancy and viral pneumonia. *J Clin Invest.* 2025;135(9).

54. Morales-Nebreda L, et al. Intratracheal administration of influenza virus is superior to intranasal administration as a model of acute lung injury. *Journal of Virological Methods.* 2014;209:116-120.

55. Vandivort TC, et al. *An Improved Method for Rapid Intubation of the Trachea in Mice.* Vol 108: 1940-087X; 2016.

56. Weinberg SE, et al. Mitochondrial complex III is essential for suppressive function of regulatory T cells. *Nature.* 2019;565(7740):495-499.

57. Misharin AV, et al. Monocyte-derived alveolar macrophages drive lung fibrosis and persist in the lung over the life span. *J Exp Med.* 2017;214(8):2387-2404.

58. Subramanian A, et al. Gene set enrichment analysis: a knowledge-based approach for interpreting genome-wide expression profiles. *Proc Natl Acad Sci U S A.* 2005;102(43):15545-15550.

59. Godec J, et al. Compendium of Immune Signatures Identifies Conserved and Species-Specific Biology in Response to Inflammation. *Immunity.* 2016;44(1):194-206.

60. McGrath-Morrow SA, et al. DNA methylation regulates the neonatal CD4(+) T-cell response to pneumonia in mice. *J Biol Chem.* 2018;293(30):11772-11783.

61. Liu Q, et al. Novel enzyme-based reduced representation method for DNA methylation profiling with low inputs. *Nucleic Acids Res.* 2025;53(12).

62. Walter JM, et al. Multidimensional assessment of alveolar T cells in critically ill patients. *JCI Insight.* 2018;3(17).

Figure 1

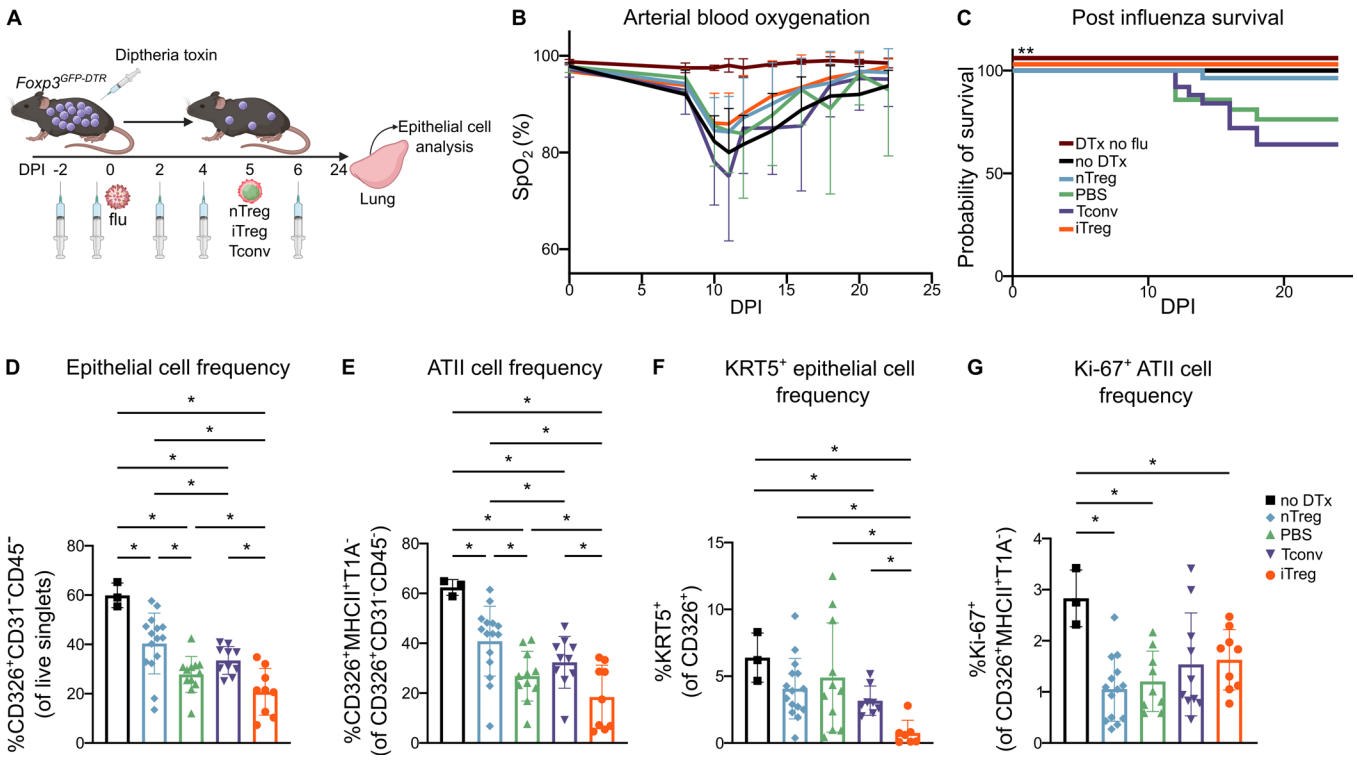

Figure 1: *Adoptive transfer of iTregs promotes survival following viral pneumonia.*

Foxp3$^{GFP\text{-}DTR}$ mice were treated with diphtheria toxin (DTx) every 48 hours beginning two days prior to inoculation with 6.5 PFUs of influenza A/WSN/33 H1N1 virus and on 5 DPI received retroorbital adoptive transfer of 1x10^6 nTregs, iTregs, conventional T cells (Tconv) or PBS. Additional controls received DTx but no influenza inoculation (DTx no flu) or influenza inoculation but no diphtheria toxin (no DTx). **(A)** Schematic of experimental design. **(B)** Mice were followed over time for arterial oxyhemoglobin saturation (SpO_2) measured via dorsal collar clip **(C)** Survival of mice that received indicated treatments. **(D-G)** Mice were euthanized on 24 DPI and lungs were analyzed by flow cytometry for **(D)** frequency of epithelial, CD326$^+$CD31$^-$CD45$^-$ cells **(E)** frequency of ATII, CD326$^+$MHCII$^+$T1A$^-$ cells **(F)** frequency of KRT5$^+$CD326$^+$ epithelial cells **(G)** frequency of Ki-67$^+$CD326$^+$MHCII$^+$T1A$^-$ cells. Data from recipients of iTregs derived from post-caval lobe, data from recipients of all other groups derived from whole lung suspensions. (**B**, DTx no flu n=4, no DTx n=6, nTreg n=11, PBS n=9, Tconv n=12, iTreg n=18; **C**, DTx no flu n=4, no DTx n=9, nTreg n=27, PBS n=21, Tconv n=25, iTreg n=18; **D-E**, no DTx n=3, nTreg n=15, PBS n=11, Tconv n=10, iTreg n=9; **F**, no DTx n=3, nTreg n=15, PBS n=11, Tconv n=8, iTreg n=7; **G**, no DTx n=3, nTreg n=14, PBS n=9, Tconv n=10, iTreg n=9). Data in **B** generated from four independent experiments. Data in **C** generated

from five independent experiments. Data in **D-G** generated from four independent experiments. Survival curve **(C)** *p*-value was determined using the log-rank (Mantel-Cox) test, $**p < 0.005$. Data presented as mean and SD with $* q < 0.05$ according to multiple Mann-Whitney tests and correcting for multiple comparisons using the two-stage linear step-up procedure of Benjamini, Krieger, and Yekutieli with Q = 5% **(D-G)**.

Figure 2

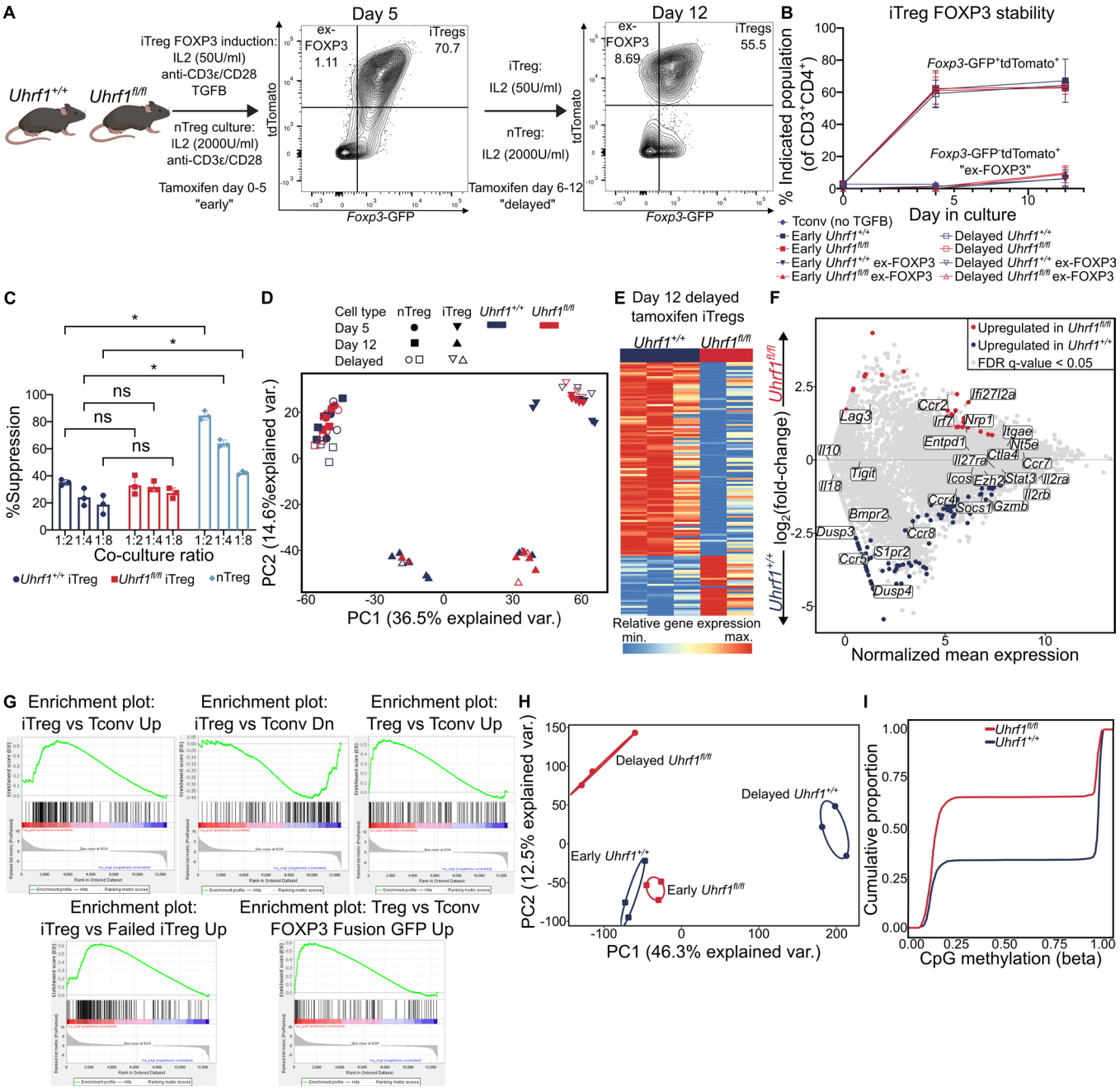

Figure 2: *UHRF1 is dispensable for iTreg FOXP3 expression and suppressive capacity but is required for transcriptional and epigenetic stability in vitro.*

(A-D) Natural and induced Tregs derived from *Uhrf1*$^{+/+}$ and *Uhrf1*$^{fl/fl}$ mice were exposed to tamoxifen to delete UHRF1 from days 0-5 ("early") or days 6-12 ("delayed") of culture then harvested on day 5 and day 12 for flow cytometry and RNA-seq analysis. **(A)** Schematic. **(B)** Frequency of *Foxp3*-GFP^{+}tdTomato^{+} iTregs and *Foxp3*-GFP^{-}tdTomato^{+} (ex-FOXP3)

cells. **(C)** Percent suppression of $CD4^+CTV^+$*Foxp3*-GFP^- splenic responder T cells co-cultured for 72 hours at indicated ratios of experimental Tregs. **(D)** PCA of 6,978 differentially expressed genes, identified from ANOVA-like testing with FDR q < 0.05. Ellipses represent normal contour lines with 1 standard deviation probability. **(E-I)** Induced Tregs derived from *Uhrf1*$^{+/+}$ and *Uhrf1*$^{fl/fl}$ mice were exposed to tamoxifen to delete UHRF1 from days 6-12 ("delayed") of culture then harvested on day 12 for RNA-seq and DNA methylation analysis. **(E)** K-means clustering of 127 genes with an FDR q < 0.05 with k = 2. **(F)** MA plot comparing gene expression between groups. Genes of interest are annotated. **(G)** Enrichment plots of gene sets (p < 0.05, FDR q < 0.25) generated through GSEA pre-ranked testing of the expressed genes. **(H)** PCA of 81,179 differentially methylated cytosines identified from ANOVA-like testing with FDR q < 0.05. Ellipses represent normal contour lines with 1 standard deviation probability. **(I)** Cumulative distribution function plot of differentially methylated cytosines expressed as β scores, with 0 representing unmethylated and 1 representing fully methylated; a shift in the cumulative distribution function up and to the left represents relative hypomethylation. (**B**, n=3 per group; **C**, n=3 per group; **D-I**, n=2 for *Uhrf1*$^{fl/fl}$*, n=3 for Uhrf1*$^{+/+}$). **B-C** representative of three independent biological replicates. Ns; not significant, *q < 0.05 according to two-way ANOVA with two-stage linear step-up procedure of Benjamini, Krieger, and Yekutieli with Q = 5 **(C)**.

Figure 3

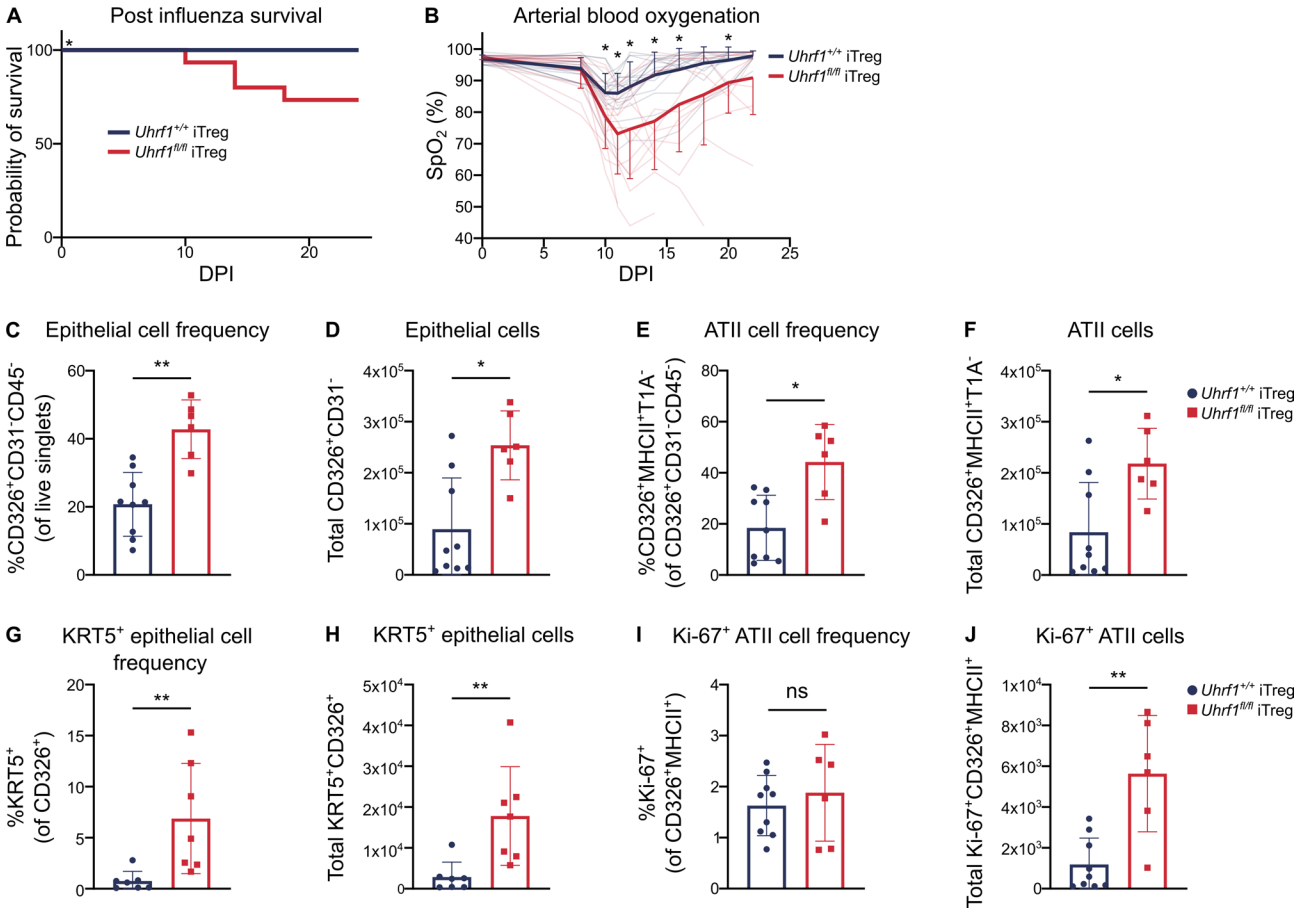

Figure 3: Loss *of UHRF1 is sufficient to impair repair capabilities of iTregs during viral pneumonia.*

Foxp3$^{GFP\text{-}DTR}$ mice were treated with DTx every 48 hours beginning two days before inoculation with 6.5 PFUs of influenza A/WSN/33 H1N1 virus, and then received retroorbital adoptive transfer of 1x10^6 *Uhrf1*$^{fl/fl}$ or *Uhrf1*$^{+/+}$ iTregs on 5 DPI as in Figure 1. iTregs were treated with tamoxifen from culture day 0 to day 3 and harvested for adoptive transfer on culture day 5. Mice were euthanized 24 DPI and lungs were analyzed by flow cytometry. Epithelial cell data is derived from the post caval lobes. **(A)** Survival of *Foxp3*$^{GFP\text{-}DTR}$ mice that received *Uhrf1*$^{+/+}$ or *Uhrf1*$^{fl/fl}$ iTregs. (**B**) Arterial oxyhemoglobin saturation (SpO_2) over time in mice from A. **(C)** CD326$^+$CD31$^-$ cell frequency and **(D)** total number. **(E)** CD326$^+$MHCII$^+$T1A$^-$ cell frequency and **(F)** total number. **(G)** KRT5$^+$CD326$^+$ cell frequency and **(H)** total number. **(I)** Ki-67$^+$CD326$^+$MHCII$^+$ cell frequency and **(J)** total number. (**A-B**, *Uhrf1*$^{+/+}$ iTreg recipients n=18, *Uhrf1*$^{fl/fl}$ iTreg recipients n=15; **C-F**, *Uhrf1*$^{+/+}$ iTreg recipients n=9, *Uhrf1*$^{fl/fl}$ iTreg recipients n=6; **G-H**, *Uhrf1*$^{+/+}$ iTreg recipients n=7, *Uhrf1*$^{fl/fl}$ iTreg recipients n=6; I-J, *Uhrf1*$^{+/+}$ iTreg recipients n=9, *Uhrf1*$^{fl/fl}$ iTreg recipients n=6.) Survival curve **(A)** *p*-value was determined using log-rank (Mantel-Cox)

test, *$p < 0.05$. *$p < 0.05$ or * $q < 0.05$ according to mixed-effects model (REML) with two-stage linear step-up procedure of Benjamini, Krieger, and Yekutieli with Q = 5% **(B)**. Data presented as mean and SD with *$p < 0.05$ according to Mann-Whitney U test **(C-J)**, Ns; not significant. Data from recipients of *Uhrf1*$^{+/+}$ iTregs are re-presented from results shown in Figure 1 and were generated in contemporaneous experiments as the data generated from mice which received UHRF1-deficient mice (*Uhrf1*$^{fl/fl}$). Data in **A-B** generated from four independent experiments. Data in **C-J** generated from two independent experiments.

Figure 4

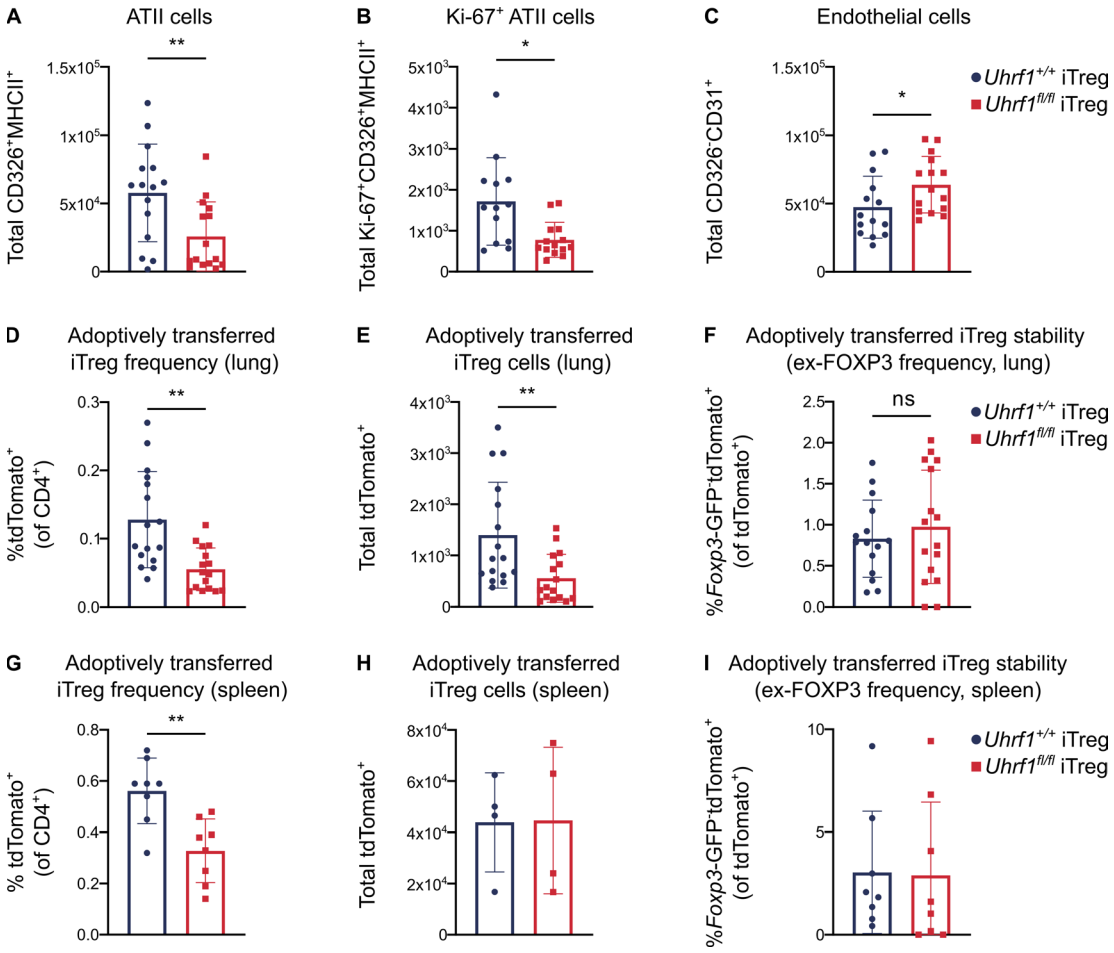

Figure 4: *UHRF1-deficient iTregs promote an insufficient tissue-protective response during peak lung injury.*

Foxp3$^{GFP\text{-}DTR}$ mice were treated with DTx every 48 hours beginning two days prior to inoculation with 6.5 PFUs of influenza A/WSN/33 H1N1 virus and received retroorbital adoptive transfer of 1x10^6 *Uhrf1*$^{fl/fl}$ or *Uhrf1*$^{+/+}$ iTregs on 5 DPI. iTregs were treated with tamoxifen from day 0-3 of culture and harvested for adoptive transfer on culture day 5. Recipient mice were euthanized 11 DPI and lungs and spleen were analyzed by flow cytometry. Epithelial cell data is derived from the post caval lobes. Transferred iTreg quantification is derived from the remaining lung lobes. **(A)** Total number of ATII cells (n=15 per group). **(B)** Total number of Ki-67$^+$ ATII cells (*Uhrf1*$^{+/+}$ iTregs n=13; U*hrf1*$^{fl/fl}$ iTregs n=14). **(C)** Total number of CD326$^-$ CD31$^+$ (endothelial) cells (*Uhrf1*$^{+/+}$ iTregs n=14; U*hrf1*$^{fl/fl}$ iTregs n=15). **(D)** Frequency of tdTomato$^+$ cells in lung (n=16 per group). **(E)** Total number of tdTomato$^+$ cells in lung (n=16 per group). **(F)** Frequency of *Foxp3*-GFP$^-$tdTomato$^+$ (ex-FOXP3) cells (*Uhrf1*$^{+/+}$ n=15; *Uhrf1*$^{fl/fl}$ n=16) in lung. **(G)** Frequency of tdTomato$^+$ cells in spleen (n=8 per group). **(H)** Total number

of tdTomato$^+$ cells in spleen (n=4 per group). **(I)** Frequency of *Foxp3*-GFP$^-$tdTomato$^+$ cells in spleen (n=8 per group). Data presented as mean and SD. *$p < 0.05$; **$p < 0.005$; ns; not significant, according to Mann-Whitney U test. Data in **A-F and I** generated from two independent experiments. Data in **H** generated from a third independent experiment.

Figure 5

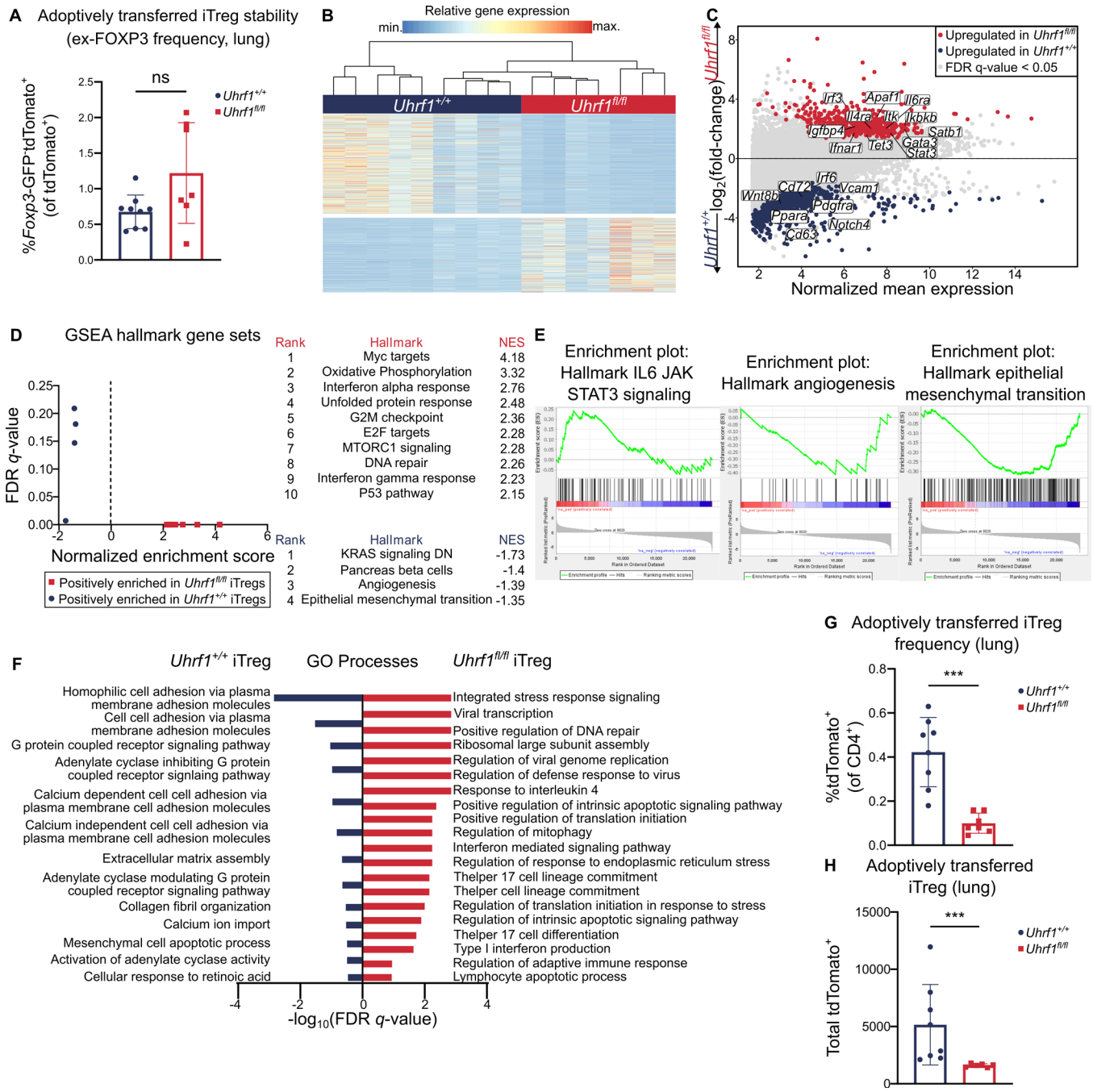

Figure 5: *UHRF1 is required for iTreg phenotypic stability and lung tissue engraftment following viral pneumonia.*

DTx treated, influenza A infected *Foxp3*$^{GFP\text{-}DTR}$ recipient mice received retroorbital adoptive transfer of 1x10^6 *Foxp3*-GFP$^+$tdTomato$^+$ *Uhrf1*$^{fl/fl}$ or *Uhrf1*$^{+/+}$ iTregs on 5 DPI. iTregs were cultured with tamoxifen from day 0-3 then harvested for adoptive transfer, as in Figure 1. Transferred *Foxp3*-GFP$^+$tdTomato$^+$ *Uhrf1*$^{fl/fl}$ or *Uhrf1*$^{+/+}$ iTregs were sorted from the lungs of recipient *Foxp3*$^{GFP\text{-}DTR}$ mice 24 DPI for quantification and profiling via bulk RNA-seq. **(A)** Frequency of *Foxp3*-GFP$^-$

tdTomato$^+$ (ex-FOXP3) cells. **(B)** K-means clustering of 1,187 genes with FDR $q < 0.05$ comparing recovered *Uhrf1*$^{+/+}$ and *Uhrf1*$^{fl/fl}$ iTregs with k = 2. **(C)** MA plot comparing gene expression of recovered *Uhrf1*$^{+/+}$ and *Uhrf1*$^{fl/fl}$ iTregs. Genes of interest are annotated. **(D)** GSEA dot plot highlighting key statistics (FDR *q*-value and normalized enrichment score or NES) and enriched gene sets. Red dots denote gene sets with a positive enrichment score or enrichment at the top of the ranked list. Blue dots denote gene sets with a negative enrichment score or enrichment at the bottom of the ranked list. **(E)** Enrichment plots of hallmark gene sets generated through GSEA pre-ranked testing of the expressed genes in *Uhrf1*$^{+/+}$ and *Uhrf1*$^{fl/fl}$ iTregs. All gene sets displayed significantly enriched with FDR q value <0.25. **(F)** Selected gene ontology (GO) processes from 945 and 105 total enriched gene sets with FDR $q < 0.25$ in *Uhrf1*$^{fl/fl}$ and *Uhrf1*$^{+/+}$ iTregs, respectively. Gene sets are annotated and ranked by $-\log_{10}$-transformed FDR *q*-value. **(G)** Frequency of tdTomato$^+$ iTregs recovered. **(H)** Total number of tdTomato$^+$ iTregs recovered. ***$p < 0.0005$, ns, not significant according to Mann-Whitney U test. (**A-F**, *Uhrf1*$^{+/+}$ n=9, *Uhrf1*$^{fl/fl}$ n=7; **G**, *Uhrf1*$^{+/+}$ n=8, *Uhrf1*$^{fl/fl}$ n=7; **H**, *Uhrf1*$^{+/+}$ n=8, *Uhrf1*$^{fl/fl}$ n=6.) Data generated from two independent experiments.

Figure 6

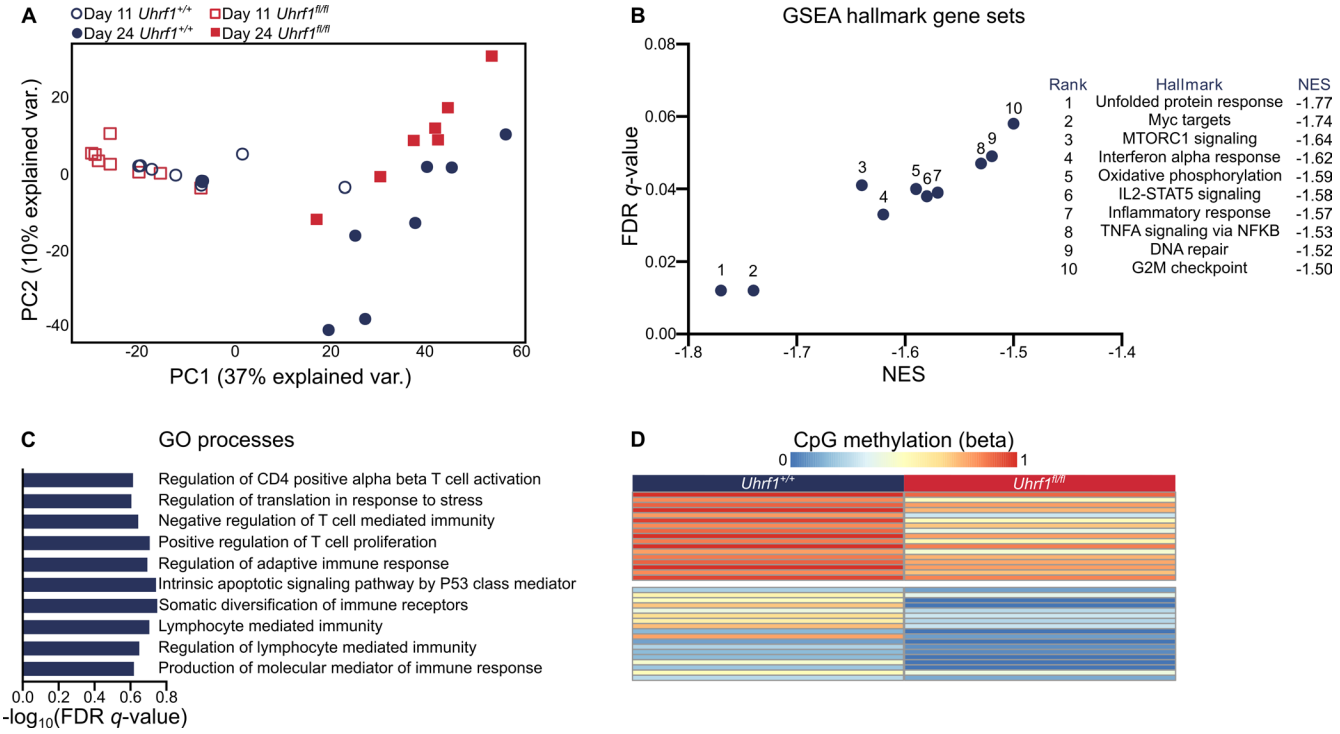

Figure 6: *Loss of UHRF1 results in delayed transcriptional changes over the course of viral pneumonia.*

Foxp3$^{GFP\text{-}DTR}$ mice were treated with DTx every 48 hours beginning two days before inoculation with 6.5 PFUs of influenza A/WSN/33 H1N1 virus and then received retroorbital adoptive transfer of 1x10^6 *Foxp3*-GFP$^+$tdTomato$^+$ *Uhrf1*$^{fl/fl}$ or *Uhrf1*$^{+/+}$ iTregs on 5 DPI as in Figure 1. iTregs were treated with tamoxifen from day 0-3 of culture then harvested for adoptive transfer on culture day 5. Adoptively transferred *Foxp3*-GFP$^+$tdTomato$^+$ *Uhrf1*$^{fl/fl}$ or *Uhrf1*$^{+/+}$ iTregs were sorted from the lungs of recipient *Foxp3*$^{GFP\text{-}DTR}$ mice 11 or 24 DPI and were compared via RNA transcriptomic and DNA methylation analysis. **(A)** PCA of 2,117 differential expressed genes identified from ANOVA-like testing with FDR $q < 0.05$. Independent biological replicates are shown. **(B)** GSEA dot plot highlighting key statistics (FDR *q*-value and normalized enrichment score or NES) and enriched gene sets for *Uhrf1*$^{+/+}$ iTregs at 11 DPI. Blue dots denote gene sets with a negative enrichment score or enrichment at the bottom of the ranked list. **(C)** Selection of representative enriched gene ontology (GO) processes from 40 total enriched gene sets with an FDR $q < 0.25$ in *Uhrf1*$^{+/+}$ iTregs at 11 DPI. Gene sets are annotated and ranked by –log$_{10}$-transformed FDR *q* value. **(D)** K-means clustering of 34 DMRs with a difference of ≥10% between *Uhrf1*$^{+/+}$ and *Uhrf1*$^{fl/fl}$

iTregs. (**A-D**, 24 DPI *Uhrf1*$^{+/+}$ iTreg recipients n=9, *Uhrf1*$^{fl/fl}$ iTreg recipients n=7; 11 DPI *Uhrf1*$^{+/+}$ and *Uhrf1*$^{fl/fl}$ iTreg recipients n=8).

Supplemental Table Legends

Supplemental Table 1. DEG lists used to generate Figures 2E-F, 5B-C, 6D, Supplemental 3A, Supplemental 7B-E. Provided as a multi-tabbed Excel file.

Supplemental Table 2. Ranked gene list used to generate Figure 2G and Supplemental Figure 3D (day 12 "delayed" *Uhrf1*$^{+/+}$ versus day 12 "delayed" *Uhrf1*$^{fl/fl}$ iTregs) against a comprehensive list of 4,872 Immunologic Signature gene sets (Figure 2G) and 50 Hallmark gene sets (Supplemental Figure 3D) housed in the Molecular Signatures Database. [provided as a tab-delimited file]

Supplemental Table 3. Ranked gene list used to generate Figures 5D-E (day 24 post influenza *Uhrf1*$^{+/+}$ versus *Uhrf1*$^{fl/fl}$ iTregs) against a comprehensive list of 50 Hallmark gene sets (Figure 5D-E) and 3,930 GO Biological Process gene sets (Figure 5F) housed in the Molecular Signatures Database. [provided as a tab-delimited file]

Supplemental Table 4. Ranked gene list used to generate Figures 6B-C (day 11 post influenza *Uhrf1*$^{+/+}$ versus *Uhrf1*$^{fl/fl}$ iTregs) against a comprehensive list of 50 Hallmark gene sets (Figure 6B) and 3,173 GO Biological Process gene sets (Figure 6C) housed in the Molecular Signatures Database. [provided as a tab-delimited file]

Supplemental Table 5. Flow cytometry fluorochromes and reagents.

Antigen/Reagent	Conjugate	Clone	Manufacturer	Catalog no.
CD4	APC-eFluor™ 780	RM4-5	Invitrogen	47-0042-82
DAPI/Cell-Impermeant Dye	N/A	N/A	Thermo Fisher Scientific	62248
CD45	FITC	30-F11	BioLegend	103107
CD31	PE	MEC 13.3	BD Pharmingen	553373
Podoplanin	PE-Cyanine7	eBio8.1.1	eBioscience	25-5381-82
CD326	BV421	G8.8	BioLegend	118225
Krt5 Krt5 Secondary Antibody	Unconjugated Alexa Fluor 488	Poly9059	BioLegend Invitrogen	905901 A11039
MHCII	BUV395	2G9	BD OptiBuild	743876
Ki-67	PerCP-eFluor 710	SolA15	eBioscience	46-5698-82
Fixable Viability Dye eFluor 506	N/A	N/A	eBioscience	65-0866-14
CD45	APC-Cy7	30-F11	BD Pharmingen	557659
CD3ε	FITC	145-2C11	Invitrogen	11-0031-85
CD4	BUV395	GK1.5	BD Horizon	565974
CD8	PECF594	53-6.7	BioLegend	100762
CD64	PE	X54-5/7.1	BioLegend	139304

CD11b	BUV737	M1/70	BD Horizon	612800
CD11c	Pe-Cy7	HL3	BD Pharmingen	558079
SiglecF	AF647 (APC)	E50-2440	BD Pharmingen	562680
Ly6G	AF 700 (A700)	1A8	BD Pharmingen	561236
CountBright™ Absolute Counting Beads	N/A	N/A	Invitrogen	C36950

Supplemental Figure 1

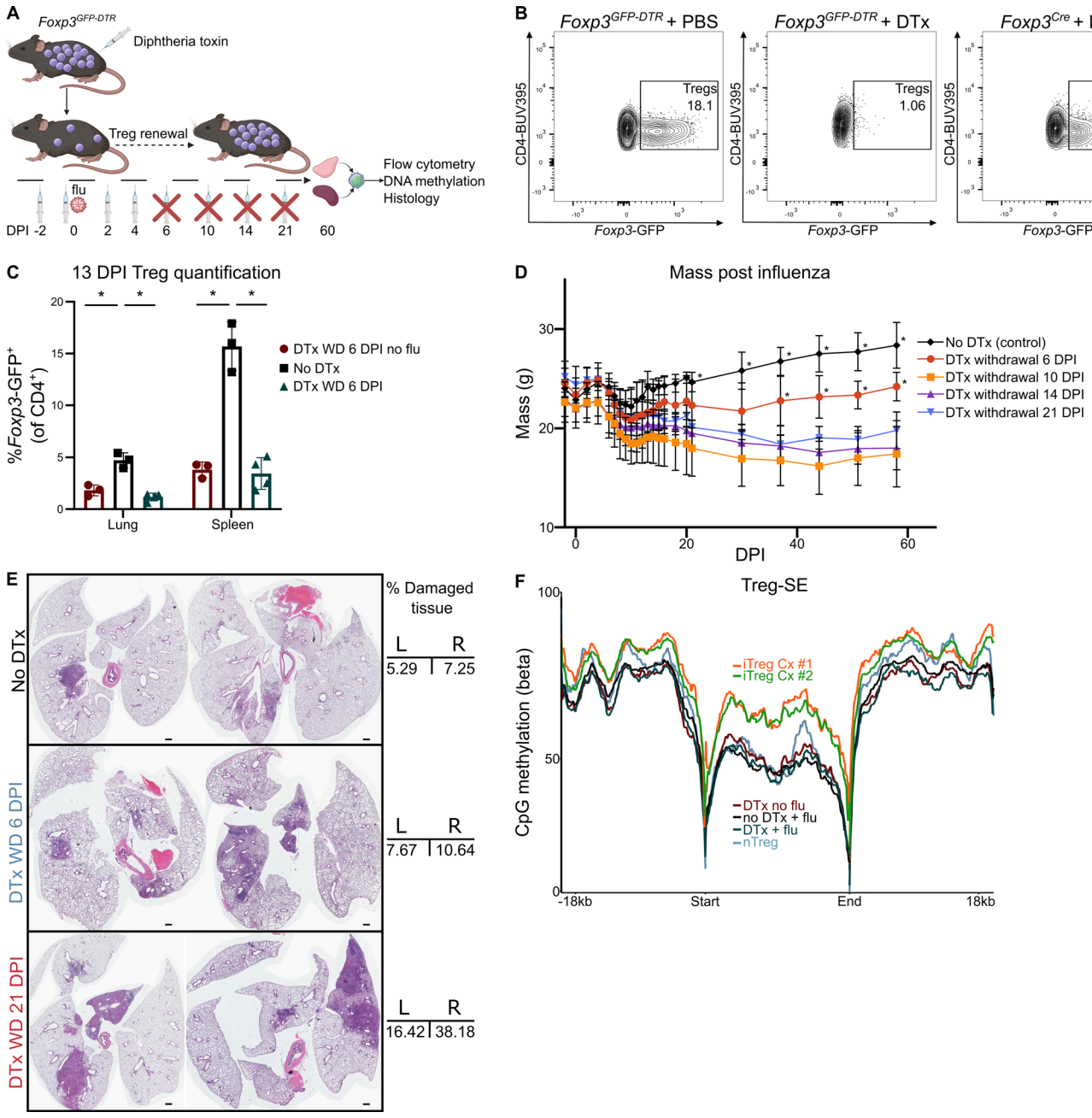

Supplemental Figure 1: *Effect of Treg renewal on recovery following influenza A virus infection.*

Foxp3$^{GFP\text{-}DTR}$ mice treated with DTx every 48 hours beginning two days prior to inoculation with 5 PFUs of influenza A/WSN/33 H1N1 virus. DTx was subsequently withdrawn (WD) on pre-specified DPIs (6, 10, 14, 21). **(A)** Schematic. **(B)** Representative flow plots of endogenous splenic CD4^{+}*Foxp3*-GFP^{+} Treg population depletion in *Foxp3*$^{GFP\text{-}DTR}$ mice following the administration of four doses of DTx (6 DPI). *Foxp3*$^{GFP\text{-}DTR}$ and *Foxp3*^{Cre} mice that received PBS and DTx, respectively,

included for comparison. **(C)** Lung and spleen *Foxp3*-GFP$^+$ Treg cell quantification in mice on 13 DPI that had DTx withdrawn on 6 DPI, (DTx WD 6 DPI, n=4), compared with mice that did not receive DTx (No DTx, n=3), or had DTx withdrawn on 6 DPI but did not receive influenza (DTx WD 6 DPI no flu n= 3). **(D)** Mass of mice described in Supplemental Figure 1A (n=4 for DTx WD 6 DPI group, n=5 for all other groups). **(E)** Representative lung histopathology (H&E staining) and percent damaged tissue at 60 DPI of control (No DTx) and DTx withdrawal (WD) mice. Original magnification x10, scale bar = 1 mm. **(F)** Metagene analysis of DNA methylation across the Treg-SE of Tregs recovered on 13 DPI from mice described in Supplemental Figure 1C compared with naïve splenic nTregs and two biological culture replicates of iTregs harvested on day 5 of culture with IL-2 and TGF-β . Independent biological replicates are shown. Data presented as mean and SD. * q < 0.05 according to one-way ANOVA with two-stage linear step-up procedure of Benjamini, Krieger, and Yekutieli with Q = 5% **(C)**.* q < 0.05 according to mixed-effects model (REML) with two-stage linear step-up procedure of Benjamini, Krieger, and Yekutieli with Q = 5% **(D)**. Data in **C-F** are each from 1 independent experiment.

Supplemental Figure 2

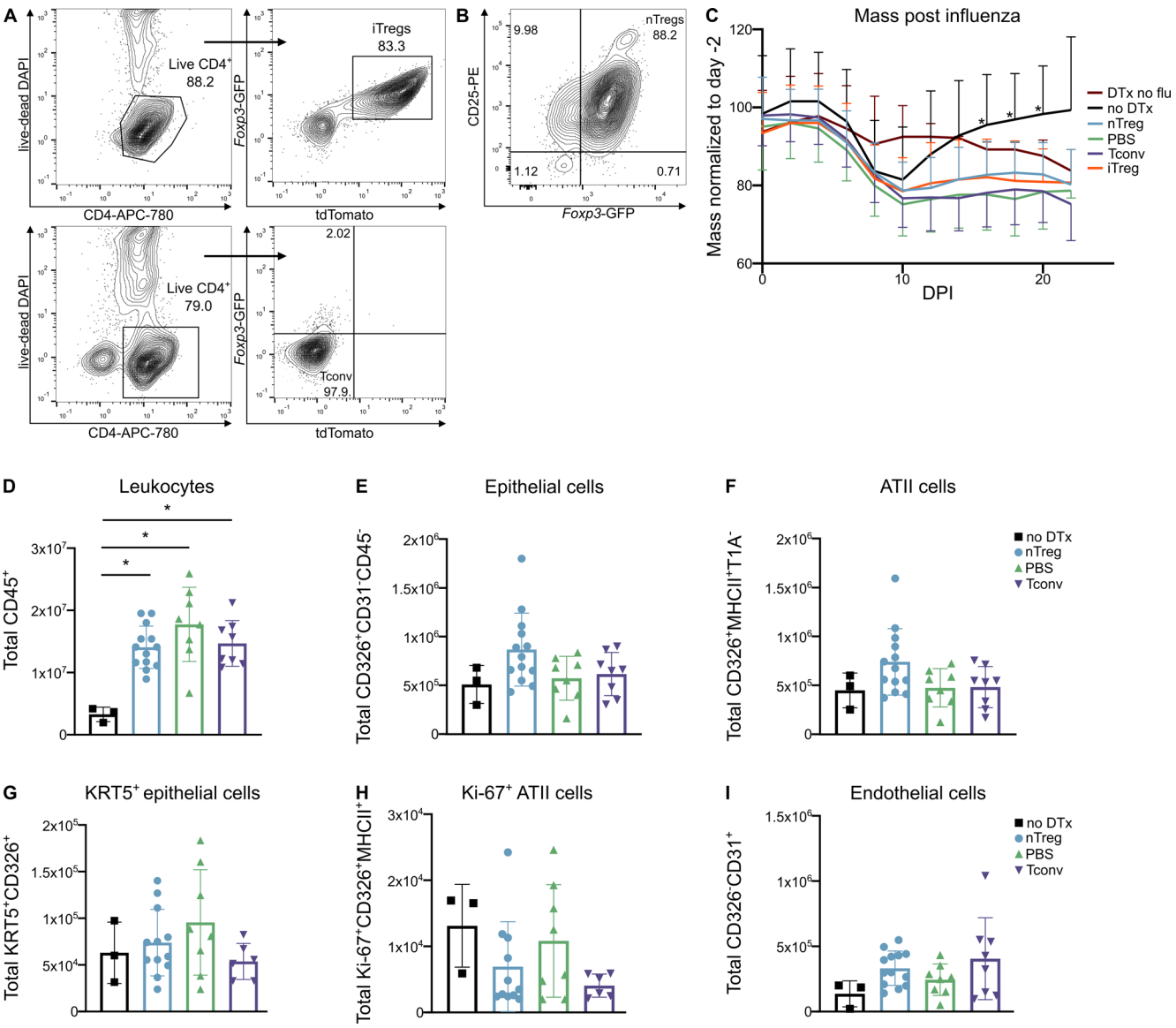

Supplemental Figure 2: *Effects of receiving DTx or no DTx.*

(A) Flow cytometry contour plots phenotyping CD4$^+$*Foxp3*-GFP$^+$tdTomato$^+$ iTreg and CD4$^+$*Foxp3*-GFP$^-$tdTomato$^-$ conventional T cell populations following 3 days of culture in the presence of αCD3ε/αCD28, IL-2, TGF-β, and tamoxifen (iTregs) or αCD3ε/αCD28 and IL-2 (Tconv). **(B)** Flow cytometry contour plot of CD4$^+$CD25$^+$*Foxp3*-GFP$^+$ nTregs isolated from the spleens of mice prior to adoptive transfer. **(C)** Mass over time of *Foxp3*$^{GFP\text{-}DTR}$ mice treated with DTx every 48 hours beginning 2 days prior to intra-tracheal inoculation of 6.5 PFU of influenza A/WSN/33 H1N1 virus, and adoptive transfer of nTreg (n=27), PBS (n=21), Tconv (n=25), or iTreg (n=18) cells on 5 DPI. Positive controls included mice that received

influenza but no DTx (no DTx, n=9) and DTx but no influenza (DTx no flu, n=3). **(D-I)** Mice were euthanized on 24 DPI and lungs were analyzed by flow cytometry for total **(D)** $CD45^+$ cells, **(E)** $CD326^+CD31^-CD45^-$ epithelial cells, **(F)** $CD326^+MHCII^+T1A^-$ ATII cells, **(G)** $KRT5^+CD326^+$ epithelial cells, **(H)** $Ki\text{-}67^+CD326^+MHCII^+$ ATII cells, and **(I)** $CD326^-CD31^+$ endothelial cells. (**D-F**, No DTx n=3, nTreg n=13, PBS n=8, Tconv n=8; **G**, No DTx n=3, nTreg n=12, PBS n=8, Tconv n=6; **H**, No DTx n=3, nTreg n=11, PBS n=8, Tconv n=6; **I**, No DTx n=3, nTreg n=13, PBS n=8, Tconv n=8). * $q < 0.05$ according to mixed-effects model (REML) with two-stage linear step-up procedure of Benjamini, Krieger, and Yekutieli with Q = 5% **(C)**. Data presented as mean and SD **(D-I)** with * $q < 0.05$ according to multiple Mann-Whitney tests and correcting for multiple comparisons using the two-stage linear step-up procedure of Benjamini, Krieger, and Yekutieli with Q = 5% **(D)**. Corresponding total cell numbers from recipients of iTregs not shown as analysis of those populations was derived from the post-caval lobe, as opposed to whole lung suspensions. Data in **C** generated from five independent experiments. Data in **D-I** generated from two independent experiments.

Supplemental Figure 3

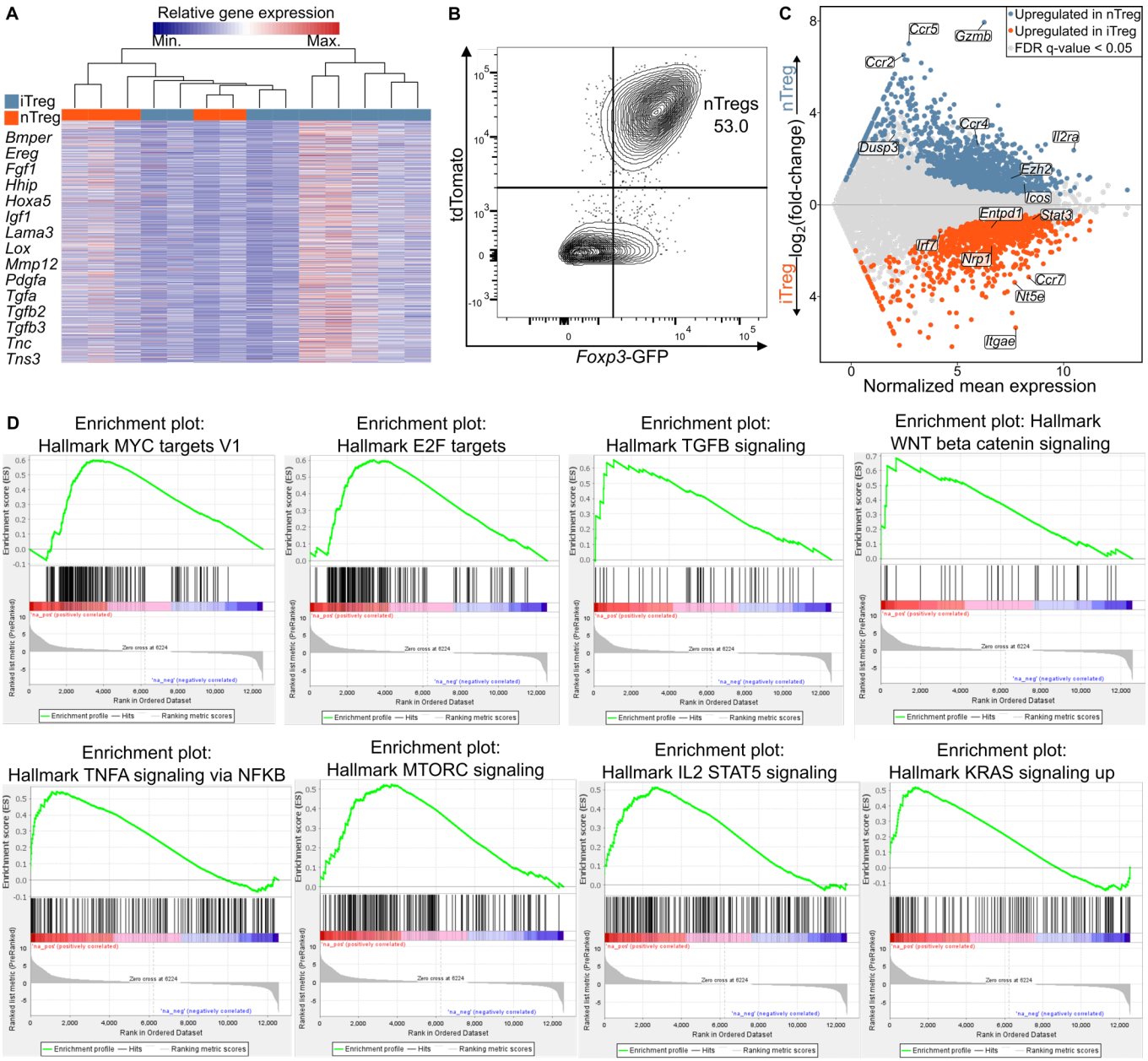

Supplemental Figure 3: *Confirmation of canonical Treg transcriptomic signature in nTregs and iTregs.*

(A) Heatmap comparing normalized counts of genes previously identified to be enriched and associated with repair function in nTregs harvested from the lungs of 8-12 week-old influenza infected *Foxp3*$^{GFP\text{-}DTR}$ mice at 60 DPI with adoptively transferred *Uhrf1*$^{+/+}$ iTregs at 24 DPI. Gene list derived from cluster II of K-means heat map shown in Figure 4 (40). Genes of interest are annotated. **(B)** Representative flow cytometry contour plot analysis of nTreg cells on day 5 of culture with tamoxifen. **(C)** MA plot comparing gene expression of *Uhrf1*$^{+/+}$ iTregs (control) with *Uhrf1*$^{+/+}$CD4^{+}*Foxp3*-GFP^{+} nTregs on day

5 of culture. Induced Tregs were generated via culture of CD4^{+}*Foxp3*-GFP^{-} T cells in the presence of αCD3ε/αCD28 coated to the plate, recombinant human IL-2 at a concentration of 50 U/ml, and TGF-β at a concentration of 10ng/ml. Natural Tregs were cultured in the presence of recombinant human IL-2 at a concentration of 2,000 U/ml and αCD3ε/αCD28 activation beads at a ratio of three beads to one Treg cell as in Figure 2A. Genes of interest are annotated. **(D)** Enrichment plots of gene sets generated through GSEA pre-ranked testing of the expressed genes of delayed *Uhrf1*$^{+/+}$ iTregs (control) and delayed *Uhrf1*$^{fl/fl}$ iTregs on day 12 of culture.

Supplemental Figure 4

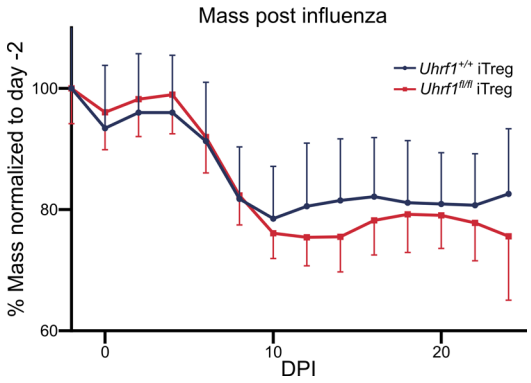

Supplemental Figure 4: iTreg *UHRF1 is dispensable for promoting mass recovery following viral pneumonia.*

Mass over time of recipient *Foxp3*$^{GFP\text{-}DTR}$ mice that were treated with DTx every 48 hours beginning two days before inoculation with 6.5 PFUs of influenza A/WSN/33 H1N1 virus and then received retroorbital adoptive transfer of 1x10^6 *Foxp3*-GFP$^+$tdTomato$^+$ *Uhrf1*$^{fl/fl}$ (n=15) or *Uhrf1*$^{+/+}$ (n=18) iTregs on 5 DPI as in Figure 1. iTregs were treated with tamoxifen from culture day 0 to day 3 and were harvested for adoptive transfer on culture day 5. Data generated from four independent experiments.

Supplemental Figure 5

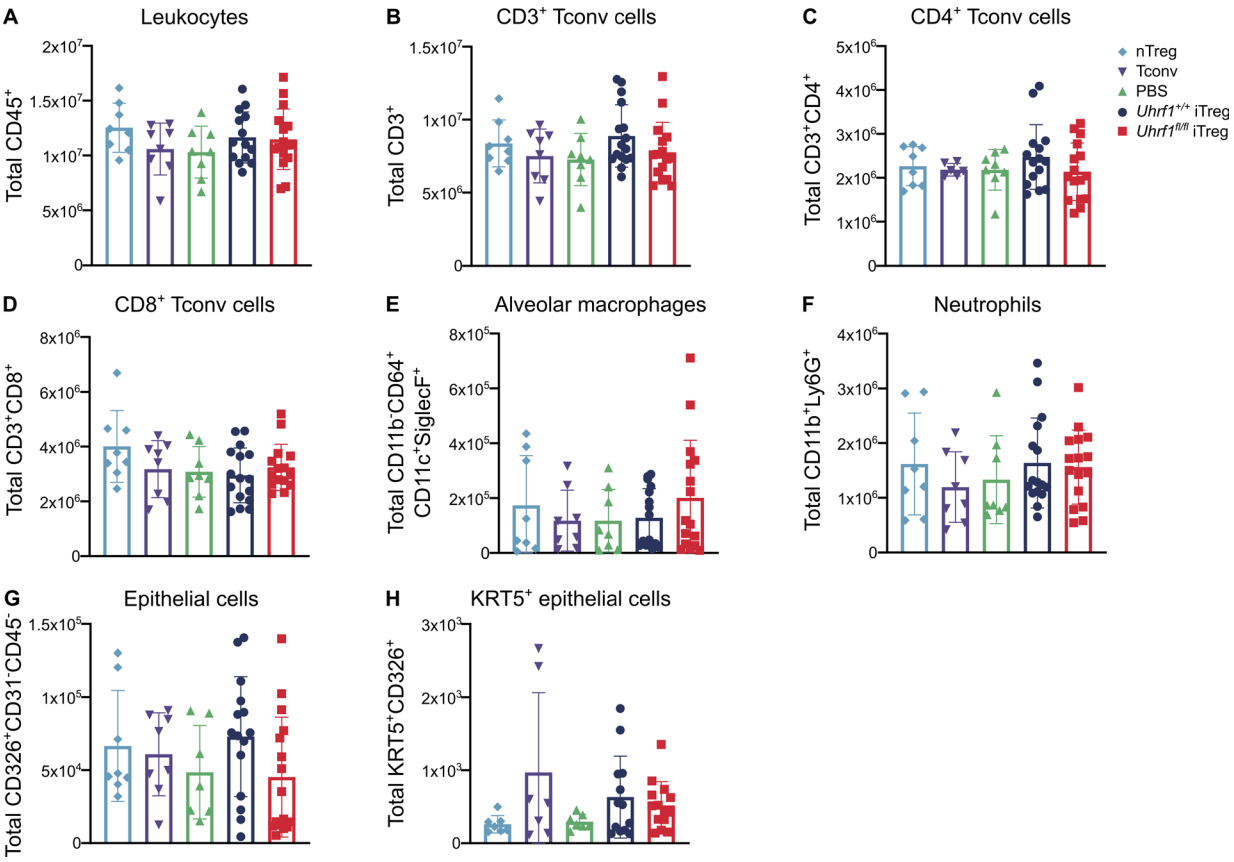

Supplemental Figure 5: *UHRF1 is dispensable for iTreg suppression of infiltrating immune cells during viral pneumonia.*

Foxp3$^{GFP\text{-}DTR}$ mice were treated with DTx every 48 hours beginning 2 days prior to inoculation with 6.5 PFUs of influenza A/WSN/33 H1N1 virus, and then received retroorbital adoptive transfer of 1x10^6 nTregs, Tconv, *Uhrf1*$^{fl/fl}$ *iTregs, Uhrf1*$^{+/+}$ iTregs, or PBS on 5 DPI. iTregs were treated with tamoxifen from culture day 0-3 and then harvested for transfer on day 5. Natural Tregs were adoptively transferred directly following isolation from the spleens and lymph nodes of mice. Recipients were euthanized on 11 DPI and lungs were analyzed by flow cytometry for total **(A)** CD45$^+$, **(B)** CD3$^+$, **(C)** CD4$^+$CD8$^-$, **(D)** CD4$^-$CD8$^+$, **(E)** CD11b$^-$CD64$^+$CD11c$^+$SiglecF$^+$, **(F)** CD11b$^+$Ly6G$^+$, **(G)** CD326$^+$CD31$^-$CD45$^-$ (epithelial), or **(H)** KRT5$^+$CD326$^+$ epithelial cells. Data in **G** and **H** derived exclusively from the post caval lobes. (**A**, nTreg (n=8), Tconv (n=8), PBS (n=8), *Uhrf1*$^{+/+}$ iTregs (n=14), U*hrf1*$^{fl/fl}$ iTregs (n=16); **B**, nTreg (n=8), Tconv (n=8), PBS (n=8), *Uhrf1*$^{+/+}$ iTregs (n=16), U*hrf1*$^{fl/fl}$ iTregs (n=16); **C**, nTreg (n=8), Tconv (n=6), PBS (n=8), *Uhrf1*$^{+/+}$ iTregs (n=15), U*hrf1*$^{fl/fl}$ iTregs (n=16); **D-E**, nTreg (n=8), Tconv (n=8), PBS (n=8), *Uhrf1*$^{+/+}$ iTregs (n=16), U*hrf1*$^{fl/fl}$ iTregs (n=15); **F**, nTreg (n=8), Tconv (n=8), PBS (n=8), *Uhrf1*$^{+/+}$ iTregs (n=16), U*hrf1*$^{fl/fl}$ iTregs (n=16); **G**, nTreg (n=8), Tconv (n=8), PBS (n=7), *Uhrf1*$^{+/+}$ iTregs (n=16), U*hrf1*$^{fl/fl}$ iTregs (n=16);

H, nTreg (n=7), Tconv (n=7), PBS (n=7), *Uhrf1*$^{+/+}$ iTregs (n=14), U*hrf1*$^{fl/fl}$ iTregs (n=14). Data presented as mean and SD. Not significant by multiple Mann-Whitney tests and correcting for multiple comparisons using the two-stage linear step-up procedure of Benjamini, Krieger, and Yekutieli with Q = 5% test. Data generated from two independent experiments.

Supplemental Figure 6

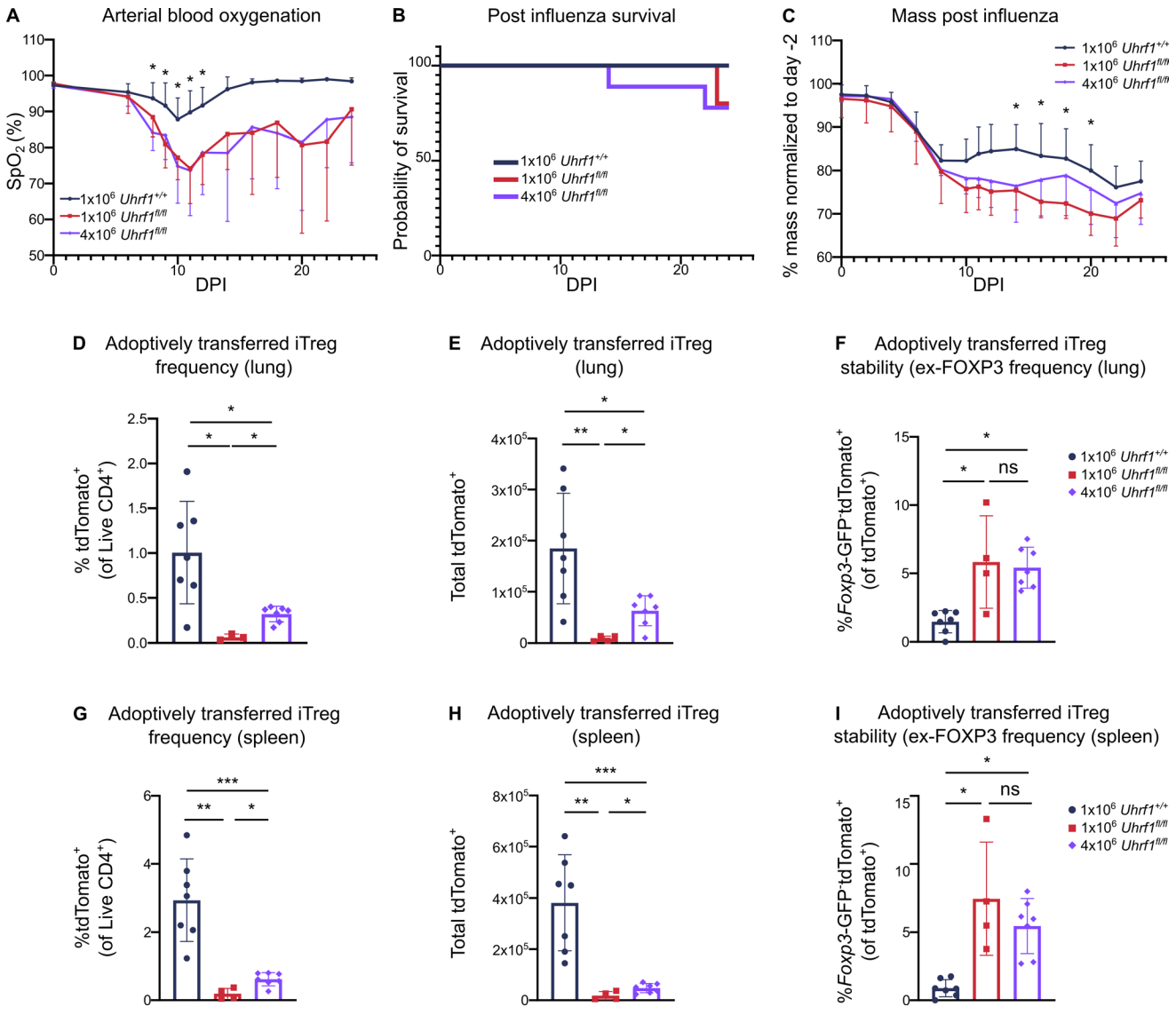

Supplemental Figure 6: Greater magnitude of *Uhrf1*$^{fl/fl}$ iTreg adoptive transfer fails to equalize tissue engraftment with *Uhrf1*$^{+/+}$ iTregs during viral pneumonia.

Foxp3$^{GFP\text{-}DTR}$ mice treated with DTx every 48 hours beginning 2 days before inoculation with 6.5 PFUs of influenza A/WSN/33 H1N1 virus, then received adoptive transfer of 1x10^6 *Uhrf1*$^{+/+}$ iTregs, 1x10^6 *Uhrf1*$^{fl/fl}$ iTregs, or 4x10^6 *Uhrf1*$^{fl/fl}$ iTregs on 5 DPI. iTregs were treated with tamoxifen from culture day 0-3, and harvested for adoptive transfer on culture day 5. Surviving mice were euthanized on 24 DPI and lungs and spleens were analyzed by flow cytometry. **(A-C)** *Foxp3*$^{GFP\text{-}DTR}$ mice that received 1x10^6 *Uhrf1*$^{+/+}$ iTregs (n=7), 1x10^6 *Uhrf1*$^{fl/fl}$ iTregs (n=5), or 4x10^6 *Uhrf1*$^{fl/fl}$ iTregs (n=9) were measured for **(A)** arterial oxyhemoglobin saturation (SpO_2), **(B)** survival, or **(C)** mass. **(D-F)** Lungs from 1x10^6 *Uhrf1*$^{+/+}$ iTregs, 1x10^6

Uhrf1$^{fl/fl}$ iTregs, or 4x10^6 *Uhrf1*$^{fl/fl}$ iTreg recipients were isolated and analyzed for **(D)** frequency of tdTomato$^+$ cells (1x10^6 *Uhrf1*$^{+/+}$ iTregs n=7*;* 1x10^6 *Uhrf1*$^{fl/fl}$ iTregs n=3; or 4x10^6 *Uhrf1*$^{fl/fl}$ iTregs n=7), **(E)** total number of tdTomato$^+$ cells (1x10^6 *Uhrf1*$^{+/+}$ iTregs n=7; 1x10^6 *Uhrf1*$^{fl/fl}$ iTregs n=4; or 4x10^6 *Uhrf1*$^{fl/fl}$ iTregs n=7) and **(F)** frequency of Foxp3$^-$tdTomato$^+$ (ex-FOXP3) cells (1x10^6 *Uhrf1*$^{+/+}$ iTregs n=7; 1x10^6 *Uhrf1*$^{fl/fl}$ iTregs n=4; or 4x10^6 *Uhrf1*$^{fl/fl}$ iTregs n=7). **(G-I)** Spleens from 1x10^6 *Uhrf1*$^{+/+}$ iTregs (n=7), 1x10^6 *Uhrf1*$^{fl/fl}$ iTregs (n=4), or 4x10^6 *Uhrf1*$^{fl/fl}$ iTregs (n=7) recipients were isolated and analyzed for **(G)** frequency of tdTomato$^+$ cells, **(H)** total number of tdTomato$^+$ cells, and **(I)** frequency of Foxp3$^-$tdTomato$^+$ (ex-FOXP3) cells. Data presented as mean and SD with * $p < 0.05$, ** $p < 0.005$, according to multiple Mann-Whitney U tests and correcting for multiple comparisons using the two-stage linear step-up procedure of Benjamini, Krieger, and Yekutieli with Q = 5%, ns, not significant **(D-I)**. * $q < 0.05$ according to mixed-effects model (REML) with two-stage linear step-up procedure of Benjamini, Krieger, and Yekutieli with Q = 5% **(A, C)**. Data in **A-I** generated from one independent experiment.

Supplemental Figure 7

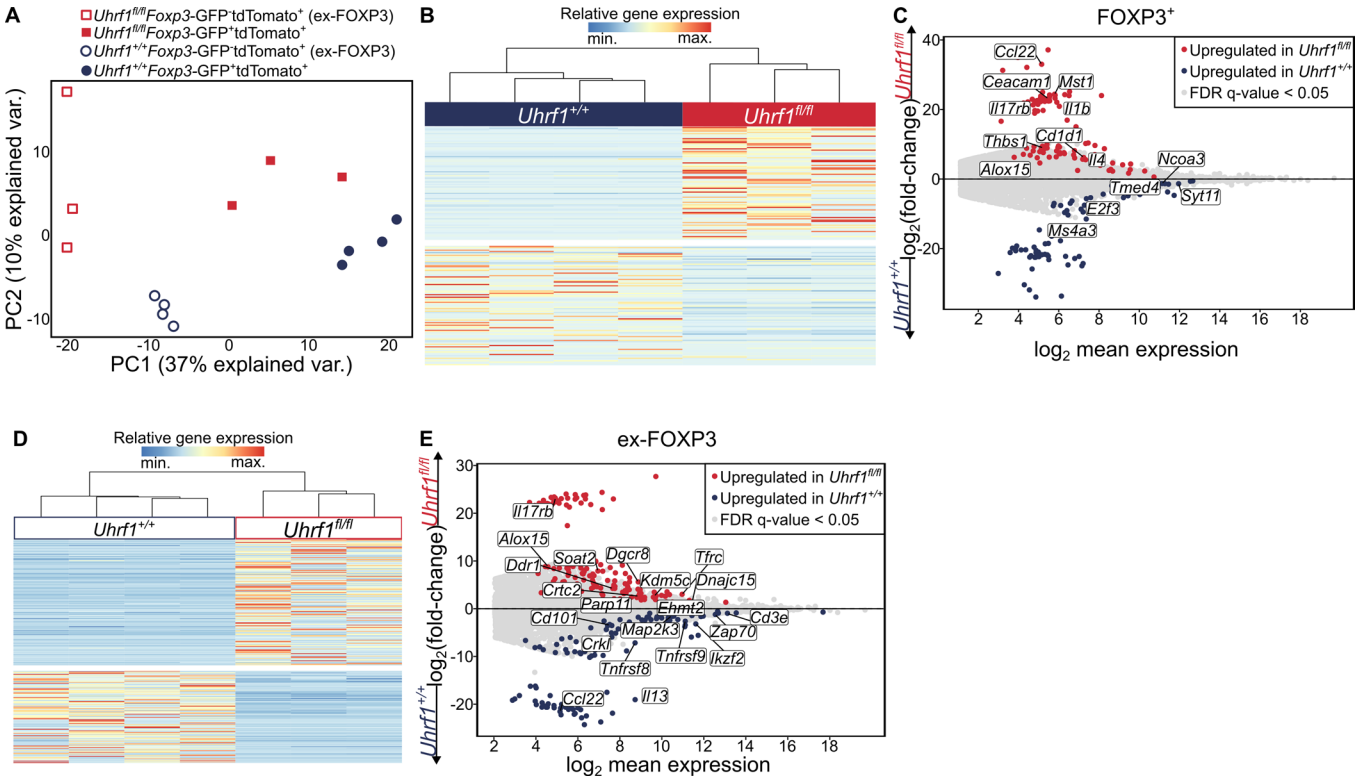

Supplemental Figure 7: *UHRF1 is required for iTreg phenotypic stability following viral pneumonia.*

Foxp3$^{GFP\text{-}DTR}$ mice treated with DTx every 48 hours beginning 2 days before inoculation with 6.5 PFUs of influenza A/WSN/33 H1N1 virus, then received adoptive transfer of 1x10^6 *Uhrf1*$^{+/+}$ iTregs (n=4) or 1x10^6 *Uhrf1*$^{fl/fl}$ iTregs (n=3) on 5 DPI. iTregs were treated with tamoxifen from culture day 0-3 and then harvested for adoptive transfer on culture day 5. On day 24 post infection *Foxp3*-GFP$^+$tdTomato$^+$ and *Foxp3*-GFP$^-$tdTomato$^+$ (ex-FOXP3) *Uhrf1*$^{+/+}$ or *Uhrf1*$^{fl/fl}$ cells were sorted from single-cell suspensions of spleens for quantification and gene expression profiling. **(A)** PCA of 457 differential expressed genes from sorted *Uhrf1*$^{+/+}$ and *Uhrf1*$^{fl/fl}$ cells harvested from the spleen 24 DPI identified from ANOVA-like testing with FDR $q < 0.05$. **(B)** K-means clustering of 183 genes with FDR $q < 0.05$ comparing FOXP3$^+$ *Uhrf1*$^{+/+}$ and *Uhrf1*$^{fl/fl}$ iTregs harvested from the spleens of *Foxp3*$^{GFP\text{-}DTR}$ mice at 24 DPI with k = 2. **(C)** MA plot comparing gene expression of adoptively transferred FOXP3$^+$ *Uhrf1*$^{+/+}$ and *Uhrf1*$^{fl/fl}$ iTregs harvested from the spleen 24 DPI. Genes of interest are annotated. **(D)** K-means clustering of 274 genes with FDR $q < 0.05$ comparing ex-FOXP3 *Uhrf1*$^{+/+}$ and *Uhrf1*$^{fl/fl}$ cells harvested from the spleens of *Foxp3*$^{GFP\text{-}DTR}$ mice at 24 DPI with k = 2. **(E)** MA plot comparing gene expression of adoptively

transferred ex-FOXP3 *Uhrf1*$^{+/+}$ and *Uhrf1*$^{fl/fl}$ cells harvested from the spleen 24 DPI. Genes of interest are annotated. Data in **A-E** generated from 1 independent experiment. Independent biological replicates are shown.

Supplemental Figure 8

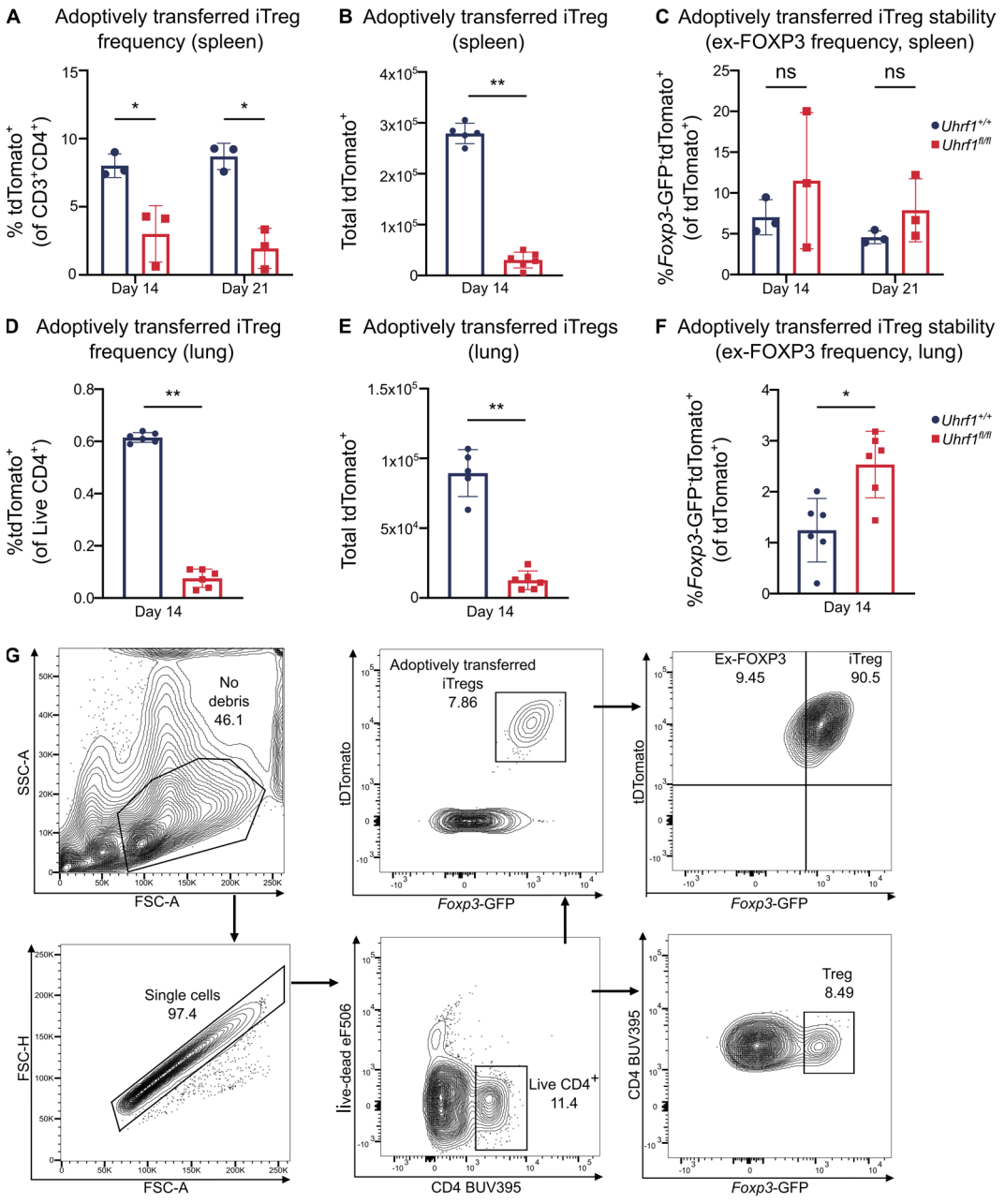

Supplemental Figure 8: *UHRF1 is required for iTreg lung and splenic tissue engraftment in the absence of viral pneumonia.*

Foxp3$^{GFP\text{-}DTR}$ mice were treated with DTx every 48 hours starting on day 0 and received retroorbital adoptive transfer of 1x10^6 *Uhrf1*$^{+/+}$ iTregs or 1x10^6 *Uhrf1*$^{fl/fl}$ iTregs on day 5. iTregs were treated with tamoxifen from culture day 0-3 and then were harvested for adoptive transfer on culture day 5. Mice were euthanized on day 14 or 21 and the spleens and lungs were analyzed by flow cytometry. **(A)** Frequency of tdTomato$^+$ cells recovered from the spleens at day 14 and day 21 of recipients of *Uhrf1*$^{fl/fl}$ or *iUhrf1*$^{+/+}$ iTregs (n=3 per group). **(B)** Total tdTomato$^+$ cells recovered from the spleen at day 14

from recipients of *Uhrf1*$^{fl/f}$ (n=6) or *iUhrf1*$^{+/+}$ iTregs (n=5). **(C)** Frequency of *Foxp3*-GFP^{-}tdTomato^{+} (ex-FOXP3) cells recovered at day 14 and day 21 from the spleens of recipients of *Uhrf1*$^{fl/fl}$ or *Uhrf1*$^{+/+}$ iTregs (n=3 per group). **(D)** Frequency of tdTomato^{+} cells recovered from the lungs at day 14 of recipients of *Uhrf1*$^{fl/fl}$ or *iUhrf1*$^{+/+}$ iTregs (n=6 per group). **(E)** Total number of tdTomato^{+} cells recovered from the lungs at day 14 of recipients of *Uhrf1*$^{fl/fl}$ (n=6) or *iUhrf1*$^{+/+}$ iTregs (n=5). **(F)** Frequency of *Foxp3*-GFP^{-}tdTomato^{+} (ex-FOXP3) cells recovered at day 14 from the lungs of recipients of *Uhrf1*$^{fl/fl}$ or *Uhrf1*$^{+/+}$ iTregs (n=6 per group). **(G)** Representative gating strategy of splenic Ex-FOXP3 population presented in Supplemental Figure 8C. Data presented as mean and SD with * $p < 0.05$ according to Mann-Whitney U test. Data in **A and C** are representative of 2 independent experiments. Data in **B and D-F** generated from 1 independent experiment.